Dynamic Stabilization of Atmospheric Single Column models

John W. Bergman and Prashant D. Sardeshmukh
NOAA-CIRES Climate Diagnostics Center
Boulder, Colorado

Submitted to *J. Climate*
Revised July 2003

Corresponding author address: John Bergman, Mail Code: R/CDC1, 325 Broadway, Boulder CO 80305-3328
E-mail: bergmanj@colorado.edu

Abstract

Single Column Models (SCMs) provide an economical framework for assessing the sensitivity of atmospheric temperature and humidity to natural and imposed perturbations, and also for developing improved representations of diabatic processes in weather and climate models. Their economy is achieved at the expense of ignoring interactions with the circulation dynamics; thus advection by the large-scale flow is either prescribed or neglected. This artificial decoupling of the diabatic and adiabatic tendencies can often cause rapid error growth in SCM integrations, especially in the tropics where large-scale vertical advection is important. As a result, SCMs can quickly develop highly unrealistic thermodynamic structures, making it pointless to study their subsequent evolution.

This paper suggests one way around this fundamental difficulty through a simple coupling of the diabatic and adiabatic tendencies. In essence, the local vertical velocity at any instant is specified by a formula that links the local vertical temperature advection to the evolution of SCM-generated diabatic heating rates up to that instant. This vertical velocity is then used to determine vertical humidity advection, and also horizontal temperature and humidity advection under an additional assumption that the column is embedded in a uniform environment. The parameters in the formula are estimated in a separate set of calculations, from the approach to equilibrium of a linearized global primitive-equation model forced by steady heat sources. As a test, the parameterized dynamics are used to predict the linear model's local response to oscillating heat sources, and found to perform remarkably well over a wide range of space and time scales. In a second test, the parameterization is found to capture important aspects of a general circulation model's vertical advection and temperature tendencies and their lead-lag relationships with diabatic heating fluctuations at convectively active locations in the tropics.

When implemented in the NCAR SCM, the dynamically coupled SCM shows a clear improvement over its uncoupled counterpart for tropical conditions observed during TOGA COARE. Coupling effectively stabilizes the SCM. As a result, short-term prediction errors are substantially reduced, the ensemble spread is reduced in ensemble runs, and the SCM is able to maintain realistic thermodynamic structures in extended runs. Such a dynamically coupled SCM should therefore be more useful not only for isolating physical parameterization errors in weather and climate models, but also for economical simulations of regional climate variability.

1. Introduction

Atmospheric single column models (SCMs) calculate the time evolution of vertical profiles of temperature and moisture in the atmosphere. They ignore interactions with the circulation dynamics, so advection by the large-scale flow is either prescribed or neglected. This simplification makes them computationally inexpensive, allowing one to explore climate change hypotheses in a variety of scenarios (e.g., Manabe and Wetherald 1967, Lee et al 1997). SCMs are also extensively used in the development and evaluation of representations of diabatic processes in weather and climate models (e.g., Stokes and Schwartz 1994; Randall et al. 1996; Moncrieff et al. 1997; Randall et al. 2003).

Unfortunately, the simplifications that make SCMs computationally efficient also introduce errors that confuse and compromise the results obtained from them. For example, temperature fluctuations in the tropics result from a relatively small imbalance between large diabatic and adiabatic tendencies. Prescribing the adiabatic tendencies decouples them from the model-generated diabatic tendencies, making it difficult for an SCM to maintain the proper balance between them (e.g., Emanuel and Zivkovic-Rothman 1999; Hack and Pedretti 2000; Bergman and Sardeshmukh 2003). Because of this, SCMs can develop grossly unrealistic thermal structures, with disastrous consequences for the subsequent development of convection and clouds. Furthermore, errors that are associated only with this decoupling can mask errors associated with the parameterized physics that one hopes to uncover using such models.

The rapid growth of large temperature errors is a common problem with SCMs (e.g., Ghan et al. 2000; Hack and Pedretti 2000; Xie et al. 2002). These errors affect both the short-time variability and the SCM's 'climate' (i.e., time-mean state) in longer-term integrations. To illustrate, Fig. 1 compares 6-hour temperature changes predicted by the National Center for Atmospheric Research (NCAR) SCM (Fig. 1a) to those observed during the 'Tropical Ocean Global Atmosphere Coupled

Ocean-Atmosphere Response Experiment' (TOGA COARE). The SCM's predicted changes are consistently greater than 0.5 K and sometimes exceed 2.0 K; in contrast, the observed changes rarely exceed 0.5 K. These short-range errors are, at least in part, symptomatic of the SCM's drift towards an unrealistic climate due to its decoupling from its environment. Figure 2 illustrates this drift with vertical profiles of time-averaged temperature errors from two 21-day SCM runs: one 'forced' by observed time-varying advection from the TOGA COARE data (solid line), and the other by the observed 21-day average advection (dashed line). In both cases, the average errors exceed 5.0 K in the lower troposphere and near the tropopause, and are much larger than the standard deviation of the observed temperature fluctuations (long dashes) over this 21-day period.

Previous researchers have used a variety of approaches to restore dynamical coupling to the SCM framework. Perhaps the simplest has been to add relaxation terms that 'nudge' the SCM's temperature and humidity towards observed profiles (e.g., Ghan et al. 1999; Lohmann et al. 1999; Randall and Cripe 1999). Sobel and Bretherton (2000) prescribed temperature to be constant above the planetary boundary layer in tropical simulations. This assumption, rationalized from observational evidence that tropical tropospheric temperature variations are small, forces the SCM to maintain a realistic thermal structure. With temperature effectively fixed, vertical velocity then replaces temperature as a prognostic variable. In some respects, these approaches are similar to the semi-prognostic approach (e.g., Lord 1982) that totally anchors the temperature and humidity to their observed values. While they all help the SCM to maintain a realistic thermal structure, to some degree they also introduce constraints on that structure that are difficult to relate to actual physical processes. Also, by construction, such approaches make it difficult to diagnose the impact of model physics on the thermal (and in some cases, the humidity) structure of the atmosphere.

Our principal goal in this paper is to develop and test a dynamically coupled SCM without such artificial constraints on the thermal and/or humidity structure. It is similar in spirit to that of Mapes (2003), who calculated adiabatic tendencies as the delayed response to the domain-averaged convective heating produced by a cloud-resolving model. In our model, vertical velocity is specified by a dynamically motivated formula that links vertical temperature advection to the time history of column diabatic heating rates. This vertical velocity is then used to determine vertical humidity advection, and finally horizontal temperature and humidity advection under an additional assumption that the column is embedded in a uniform environment. Our basic coupling formula is developed in Section 2. Its parameter values are estimated in Section 3 from the approach to equilibrium of a linearized primitive equation (PE) model forced by *steady* diabatic heat sources. In Section 4, the parameterized dynamics are tested for their ability to reproduce the same linear model's local response to *oscillating* heat sources. A second test assesses the ability of the parameterized dynamics to reproduce, given a GCM's time-varying diabatic heating field, the amplitude and phase of the vertical advection and temperature variations relative to those of the heating. Section 5 demonstrates that dynamical coupling effectively stabilizes the SCM and substantially reduces the errors in Figures 1 and 2. A summary and concluding remarks follow in section 6.

2. Model development

a. The conceptual framework

We use the NCAR SCM, which incorporates all the column physics that are represented in version CCM3.6 of the NCAR atmospheric GCM (Hack and Pedretti 2000). Typical of SCMs, it integrates prognostic equations for the vertical structures of temperature and humidity:

$$\begin{aligned} \frac{\partial \theta}{\partial t} &= A_\theta + Q \\ \frac{\partial q}{\partial t} &= A_q + S \end{aligned}, \tag{1}$$

where Q and S represent diabatic contributions to the temperature and moisture tendencies from the parameterized physics (described in Kiehl et al. 1996). The adiabatic tendencies

$$\begin{aligned} A_\theta &= -\mathbf{v} \bullet \nabla \theta - \omega \frac{\partial \theta}{\partial p} \\ A_q &= -\mathbf{v} \bullet \nabla q - \omega \frac{\partial q}{\partial p} \end{aligned} \tag{2}$$

represent advection by the large-scale flow. Traditionally, these terms are either fully specified ('revealed' forcing; Randall and Cripe 1999) or calculated from a combination of specified and predicted terms ('horizontal advective forcing'; Randall and Cripe 1999). In either case, the winds are specified, which effectively decouples the adiabatic and diabatic tendencies.

In the NCAR SCM, diabatic tendencies are determined using the temperature and humidity profiles from the previous time-step. That is, for the purpose of calculating diabatic tendencies, temperature and moisture profiles are known quantities. Similarly, for the development of our dynamical coupling, vertical profiles of temperature and humidity are treated as known.

The coupling proceeds as follows:

- Vertical temperature advection is calculated from the time history of diabatic heating Q using a formula motivated by the gravity wave response to heat sources imposed on a basic state at rest in a non-rotating atmosphere.

- The vertical pressure velocity ω is calculated from vertical temperature advection by dividing out the vertical temperature gradient. Vertical advection of moisture is then calculated from the vertical velocity and the vertical gradient of humidity.

- The relatively small horizontal advections of temperature and humidity are then calculated using continuity equations under the assumption that the column is embedded in a uniform large-scale environment. This completes the dynamical coupling.

b. A model for vertical advection

It is shown in the Appendix that the linearized primitive equations, for a basic state at rest in a non-rotating atmosphere, collapse to a set of second order equations for the time evolution of spatial Fourier modes of vertical temperature advection.

$$\begin{aligned} \frac{\partial^2 X_{mn}}{\partial t^2} + 2\gamma \frac{\partial X_{mn}}{\partial t} &= -\left(\gamma^2 + \sigma_{mn}^2\right)\left(X_{mn} - \alpha_{mn} Q_{mn}\right) \\ \alpha_{mn} &= \frac{\sigma_{mn}^2}{\gamma^2 + \sigma_{mn}^2} \end{aligned} \tag{3}$$

where X represents vertical advection, Q is the diabatic heating rate, σ is the intrinsic gravity wave frequency, and γ the coefficient of linear damping. The subscripts identify individual Fourier modes:

n is the total horizontal wavenumber, and *m* identifies vertical modes $\sin\left(\frac{m\pi z}{\Delta z}\right)$, where Δz is the depth of the troposphere. Sine functions form a complete basis for the vertical profile of vertical advection if the vertical velocity is assumed to be zero at the surface and at some upper boundary that is presumably near the tropopause. Equation (3) is isomorphic to the equation of state for a damped forced harmonic oscillator, with diabatic heating providing the forcing.

The solution to (3), for an atmosphere initially at rest, is

$$X_{mn}(t) = \frac{\alpha_{mn}\left(\gamma_{mn}^2 + \sigma_{mn}^2\right)}{\sigma_{mn}} \int_0^t e^{-\gamma_{mn}(t-t')} \sin\left[\sigma_{mn}(t-t')\right] Q_{mn}(t')\,dt' . \tag{4}$$

Formula (4) relates vertical temperature advection to the time history of diabatic heating with 3 parameters for each Fourier mode. In Sec. 3, we will estimate these parameters from the response of a PE model to steady heating and then test them on the response to oscillating heating. In anticipation of that discussion, consider solutions (4) for special cases: For steady heating $Q(t) \equiv Q_0$,

$$X(t) = \alpha Q_0 \left\{1 - e^{-\gamma t}\left[\cos(\sigma t) + \frac{\gamma}{\sigma}\sin(\sigma t)\right]\right\} \tag{5}$$

where subscripts and explicit space dependence have been dropped from the expression for convenience. The parameter α determines what fraction of the heating is balanced by advection in the steady state (i.e., as $t \to \infty$). At finite times, temperature advection oscillates about its steady state value αQ_0 and the amplitude of the oscillation decreases exponentially with time.

For oscillating heating rates

$$Q(t) = Q_0 \sin(\nu t), \tag{6}$$

the equilibrated ($t >> \gamma^{-1}$) advection also oscillates:

$$X(t) = \frac{\alpha Q_0\left(\gamma^2 + \sigma^2\right)}{2\sigma}\left[\frac{\gamma\cos(\nu t) + (\sigma+\nu)\sin(\nu t)}{\gamma^2 + (\sigma+\nu)^2} - \frac{\gamma\cos(\nu t) - (\sigma-\nu)\sin(\nu t)}{\gamma^2 + (\sigma-\nu)^2}\right]. \tag{7}$$

For strong damping ($\gamma >> \sigma, \nu$), advection is in phase with the heating

$$X(t) \to \alpha Q_0 \sin(\nu t) = \alpha Q(t). \tag{8}$$

For weak damping ($\gamma << \sigma, \nu$), there are three interesting cases. For "slow heating" ($\nu \ll \sigma$),

$$X(t) \to \alpha Q_0 \sin(\nu t). \tag{9}$$

Advection is in phase with the heating – as it is in the heavily damped case. In this case, the heating rate is slow enough to be effectively steady, allowing the advection and heating to remain in equilibrium with one another. For 'fast heating' ($\nu \gg \sigma$),

$$X(t) \to -\left(\frac{\sigma}{\nu}\right)^2 \alpha Q_0 \sin(\nu t). \tag{10}$$

The amplitude of the advection is small. For 'resonant heating' ($\nu \to \sigma$), the second term in the brackets in (7) dominates over the first because its denominator $\gamma^2 + (\sigma - \nu)^2$ is small. In that case,

$$X(t) \rightarrow -\left(\frac{\sigma}{2\gamma}\right)\alpha Q_0 \cos(\nu t)\,. \tag{11}$$

The amplitude of advection can be much larger than that of the heating and its phase relative to that of the heating shifts, being approximately 90° out of phase for $\nu = \sigma$.

c. A model for horizontal advection

The vertical temperature advection diagnosed from the history of diabatic heating allows us to calculate vertical velocity and vertical moisture advection as discussed previously. To complete the parameterized dynamics we need only to derive an expression for horizontal advection in terms of known quantities. This is accomplished under the assumption that the column is embedded in a uniform environment.

For any scalar Ψ (i.e., temperature or humidity in this context), horizontal advection can be written in terms of a flux divergence and horizontal wind divergence

$$\mathbf{v}\bullet\nabla\Psi = \nabla\bullet(\Psi\mathbf{v}) - \Psi\nabla\bullet\mathbf{v}\,. \tag{12}$$

Averaging over the horizontal area of the column and ignoring nonlinear interactions among sub-grid scale fluctuations that are presumably parameterized by SCM physics, the second term on the right-hand side can be related to the area-averaged vertical velocity via mass continuity as

$$\Psi\nabla\bullet\mathbf{v} = \Psi_i\nabla\bullet\mathbf{v} = -\Psi_i\frac{\partial\omega}{\partial p}, \tag{13}$$

where Ψ_i is the value of Ψ in the column interior.

The flux divergence term on the right-hand side of (12), $\nabla\bullet(\Psi\mathbf{v})$, can also be expressed in terms of vertical velocity. When the large-scale flow is convergent, that term represents a flux into the column:

$$\nabla\bullet(\Psi\mathbf{v}) = \Psi_o\nabla\bullet\mathbf{v} \tag{14}$$

where Ψ_o is the environmental value. This relationship is derived by considering the volume integral over a thin horizontal slice of the column and applying Gauss' theorem. Conversely, when the large-scale flow is divergent, the term represents a flux of Ψ out of the column:

$$\nabla\bullet(\Psi\mathbf{v}) = \Psi_i\nabla\bullet\mathbf{v}\,. \tag{15}$$

In either case, horizontal advection can be calculated in terms of known quantities: Ψ and ω,

$$\mathbf{v}\bullet\nabla\Psi \rightarrow \begin{cases} (\Psi_i - \Psi_o)\dfrac{\partial\omega}{\partial p} & \text{for } \nabla\bullet\mathbf{v} < 0 \\ 0 & \text{for } \nabla\bullet\mathbf{v} \geq 0 \end{cases}. \tag{16}$$

Note that the vertical profiles of temperature and humidity are the only specified environmental quantities in our dynamically coupled SCM, and are only used to determine horizontal advection. For tropical conditions, horizontal advection is a small component of the thermal and moisture budgets. In fact, we have repeated all of the coupled SCM calculations reported here neglecting horizontal advection, and found negligible impact on the results.

3. Implementation

a. Empirical determination of the parameters

Formula (4), as derived in the Appendix, is based on highly idealized dynamics in a non-rotating atmosphere. That derivation is nonetheless illuminating, and as we will see, explains much of the behavior of a more realistic atmospheric model. However, to estimate values for the parameters, we utilize calculations from a global linearized primitive equation (PE) model (20 vertical levels; horizontal truncation T42) that is capable of realistic tropical simulations over wide range of space and time scales (Bergman and Hendon 2000). Separate runs of the PE model forced by steady heating were performed for each spatial Fourier mode of heating Q_{mn}. In each case, the PE model was run from motionless initial conditions to a steady state. Vertical advection of temperature was projected onto the spatial structure of the heating to obtain a time-series that was assumed to be of the form (5) for estimating the parameters.

$$P_{mn}(t) = \frac{\int_V X(\lambda,\phi,z,t)Q(\lambda,\phi,z)dV}{\int_V Q^2(\lambda,\phi,z)dV} = \frac{X_{mn}(t)}{Q_{mn}} = \alpha_{mn}\left\{1 - e^{-\gamma_{mn}t}\left[\cos(\sigma_{mn}t) + \frac{\gamma_{mn}}{\sigma_{mn}}\sin(\sigma_{mn}t)\right]\right\}, \quad (17)$$

where $P_{mn}(t)$ is the projection of vertical advection onto the heating and the integral is performed over the volume V of the atmosphere. The spatial dependence of X and Q within the volume integrals of (17) involves only a single Fourier mode that is common to both the numerator and the denominator; hence the trivial simplification of that ratio. The parameters α_{mn}, γ_{mn}, and σ_{mn}, for each Fourier mode were obtained from (17) using the Levenberg-Marquardt method for non-linear parameter fitting (Press et al. 1989).

Figure 3 displays the parameters so estimated (open circles) as functions of zonal wavenumber for vertical modes m = 1, 4, and 10. For these calculations, the spatial structure of the heating was specified by Fourier modes in the zonal and vertical; the meridional structure was specified to be Gaussian with width 30°, centered on the equator. Analytic values for α and σ, which are based on idealized calculations in the Appendix (A.6) assuming a mean tropospheric temperature of 250 K, a tropospheric lapse rate of 6.5 K km^{-1}, and damping rate of (16 days)$^{-1}$, are displayed as dashed lines in Fig. 3. From these calculations, it is evident that α = 1 for all but global scales. At large zonal wavenumbers (small horizontal scales), the intrinsic frequency σ from the PE model agrees very well with the analytic value. On the other hand, the damping parameter γ^{-1} has values on the order of hours, quite different from the linear damping specified in the PE model, (16 days)$^{-1}$. That is, the additional realism of the 3-dimensional PE model alters the effective damping timescale from the idealized non-rotating calculations in the Appendix, but not the steady state fraction α or the intrinsic frequency σ.

b. A first-order approximation

The parameterized dynamics discussed so far are based on a second-order (i.e., a harmonic oscillator) relationship between vertical advection and diabatic heating. Such a relationship, for a specified horizontal scale (i.e., a single horizontal wave number) carries the implication that the heating is associated with globally-coherent wave activity. In reality, however, the horizontal structure of convection is rarely dominated by a single wave but rather represents a wave packet. These packets contain a superposition of waves that experience phase interference, which localizes the heating (e.g., Ricciardulli and Sardeshmukh 2002) and reduces resonant amplification. In light of this, we consider a simpler, first-order, approximation for the parameterized dynamics. It is not only simpler to

implement, but as we will see, actually outperforms the second order model for heating with Gaussian horizontal structures, while retaining interesting ties to gravity wave dynamics.

Similar to the approach of Mapes (2003), the first-order model represents exponential relaxation of temperature advection to the diabatic heating:

$$\frac{\mathrm{d}X}{\mathrm{d}t} = -\frac{1}{\tau}\left(X - \alpha Q\right) \tag{18}$$

where τ is the relaxation time scale and, as before, α is the fraction of the diabatic heating rate that is balanced by advection in the steady state limit. For an atmosphere initially at rest, (18) has the solution

$$X(t) = \frac{\alpha}{\tau}\int_0^t e^{\frac{t'-t}{\tau}} Q(t')\mathrm{d}t', \tag{19}$$

which for steady heating $Q(t) = Q_0$ reduces to

$$X(t) = \alpha Q_0\left(1 - e^{-\frac{t}{\tau}}\right). \tag{20}$$

As with the second-order model, the parameters are determined for each spatial Fourier component from an empirical fit of the response in the linearized PE model to (20). Figure 4 displays the values of α (Fig. 4a) and τ (Fig. 4b) as functions of zonal wavenumber for the same vertical modes shown in Fig. 3. For all but global modes, α is close to 1.0 as for the second order model. The relaxation time τ behaves much like the gravity wave timescale σ^{-1}, nearly matching the analytic values for that quantity. It might at first seem puzzling that the adjustment timescale is related to the intrinsic frequency of the second order model and not the damping rate. However, for small horizontal scales the oscillating period is shorter that the damping timescale. In that case, advection 'adjusts' to constant diabatic heating in one quarter of a cycle for an atmosphere initially at rest. After that time the advection can be considered to be oscillating about its steady state value. Finally, α and τ are not very sensitive to details of the assumed horizontal heating structure (i.e., the curves flatten out in Fig. 4) at small horizontal scales (e.g., less that $\sim 20^\circ$). This important feature of the first order dynamics means that our dynamical coupling depends mostly on the vertical structure of the heating, which is known in the SCM framework, and is not sensitive to its horizontal structure, which is not known. Thus a single specified horizontal structure is able to represent dynamical interactions over a wide range of horizontal scales. In particular, for the tropics, where the decorrelation distance for convective activity is on the order of a hundred kilometers (e.g., Ricciardulli and Sardeshmukh 2002), parameters based on a single horizontal structure can represent a substantial fraction of the observed variance.

4. Validation of the parameterized dynamics

We are now in a position to assess how well our dynamical parameterization captures local variations of vertical advection and temperature given only local variations of diabatic heating and mean environmental fields. Tests are performed first with the linear PE model and then with a GCM. In the PE model, we can control the space-time structure of the specified heating, and investigate to what extent the parameterized dynamics are more accurate at some scales than others. In contrast, we cannot directly control the heating in a GCM. However, it is more realistic; nonlinear evolution on multiple scales presents the dynamical parameterization with a more relevant and perhaps harder test. Also, remotely-forced disturbances can interfere with the local balance between diabatic heating and

adiabatic cooling posited in our coupling formula, presenting another challenge to the dynamical parameterization.

a. Tests with idealized heating in the linear PE model

In Sec. 3, values of the parameters were determined from the transient adjustment of local vertical advection to *steady* diabatic heating rates. Here, we present results from tests conducted with *oscillating* heating rates. Two sets of calculations were performed. In the first set, the horizontal structure of the heating was specified to be 'wavy' (i.e., sinusoidal; wavenumber k = 20) in the zonal direction and Gaussian in the meridional direction (width 30°). The second set specified a Gaussian zonal heating structure

$$Q(\lambda) = Q_0 e^{-\left(\frac{2\lambda}{\Lambda}\right)^2}, \tag{21}$$

where λ denotes longitude and Λ the zonal width of the heating in degrees. For these calculations, both the zonal and meridional widths were specified to be 9°, and thus parameters α, γ, and σ for these tests were chosen using an effective wavenumber

$$k_{eff} = \frac{360°}{\pi\Lambda} \approx 13. \tag{22}$$

Given the conceptual framework for the coupled SCM (i.e., that the column is embedded within a uniform region) a Gaussian horizontal structure exhibits the same radial symmetry in a horizontal plane as the coupled SCM. Such a structure, therefore, fits the context of dynamical coupling for a single column model better than a wavy heating structure. The test calculations were performed for a range of vertical structures (m = 1, 2, 4, and 8) and oscillation periods (3, 6, and 12 hr; 1, 2, 4, 8, and 16 days).

Figure 8 summarizes the results of these tests in terms of rms advection errors (normalized by the amplitude of the heating). Errors are displayed as functions of $\log\left(\frac{\nu}{\sigma}\right)$, where ν is the heating frequency and σ the intrinsic gravity wave frequency, which allows easier depiction of errors for fast heating ($\nu > \sigma$), slow heating ($\nu < \sigma$), and near resonant heating ($\nu \approx \sigma$). The errors are largest near resonance ($\log\left(\frac{\nu}{\sigma}\right) \approx 0$), and decrease to smaller values in both the fast limit, in which vertical advection is small, and the slow limit, in which vertical advection tracks fluctuations of diabatic heating.

In terms of rms error, the performance of the second order dynamics is comparable for wavy heating (Fig. 5a) and Gaussian heating (Fig. 5b). However, there appears to be a marked improvement when the first order dynamics are used to estimate the response to Gaussian heating (Fig. 5c), particularly near resonance. To further investigate the resonant case, Fig. 6 shows the vertical structure of vertical advection over one cycle of the heating for a particular case (m =1; 12 hour period). A phase of 0° in these figures represents the time of maximum heating rate. The local response of the PE model to wavy heating (Fig. 6a) displays several features that are expected near resonance: a large amplification (the amplitude of the response is 45 K day^{-1} for a heating rate of 5 K day^{-1}) and a modest phase shift of the advection with respect to the heating. In addition to the forced tropospheric response, there is a strong response in the upper atmosphere (above 100 mb) due to wave propagation into low-density air. For Gaussian heating, vertical advection from the PE model (Fig. 6b) also experiences a phase shift, but the amplitude of the response is much smaller than for wavy heating due to the phase interference that is associated with wave packets.

The parameterized dynamics (Figs. 6c and 6d) actually perform well in this difficult test despite the large rms errors in Fig. 5. The second order dynamics capture the phase shift and amplification for wavy heating in the troposphere, while the first order dynamics reproduce the phase shift and the small amplitude response (relative to that of the wavy response) for Gaussian heating. The parameterized dynamics do not produce wave propagation away from the heat source, and so cannot replicate the response of the PE model in the upper atmosphere.

b. Direct comparisons to GCM data

For this test, one month of simulated hourly heating rates, temperature, and winds from the NCAR GCM (version CCM3.10 with T42 horizontal resolution and 18 vertical levels) were obtained. Given the local hourly GCM heating rates as input, the first order dynamical parameterization was then used to calculate the hourly evolution of vertical temperature advection and temperature for each low-latitude grid cell. These parameterized variations were then compared with corresponding variations in the GCM simulation.

Figure 7 compares the evolution of vertical advection from (a) the GCM with (b) the parameterized dynamics for twenty days at a convectively-active location in the equatorial west Pacific. This location was not chosen as a "best case", but rather to illustrate two important features of the parameterized dynamics: (1) Its systematic failure to reproduce the dynamical response above 200 mb, which was also evident in the PE model calculations (e.g., Fig. 6), and (2) The relative smoothness of the parameterized advection compared to the GCM advection, which results in the loss of some small-scale features.

Neglecting the values above 200 m, the pattern correlation between Figs. 7a and 7b is 0.59. This value serves as a reference for similar correlations calculated for all GCM grid points between 45° S and 45° N, shown in Fig. 8a. The correlations are 0.5 or greater (shaded regions in Fig. 8a) at locations where convection is active (shaded regions in Fig. 8b). That is, the dynamical parameterization works well in regions of strong heating, in which the average correlation between the parameterized advection and GCM advection is about 0.7. Outside of such regions, remote disturbances apparently have a stronger influence on local dynamics.

c. Statistical comparisons to GCM data

The close agreement between the parameterized and GCM-simulated vertical advection at convectively active locations justifies the use of parameterized dynamics at those locations. Note however that a perfect hour-by-hour match of the variations is neither expected nor required for our parameterization to be useful. It is sufficient that the overall statistics of the parameterized dynamical variations (including lead-lag correlations) be consistent with those of the diabatic heating, and the temperature changes resulting from the small imbalance between them be of realistic magnitude. There are bound to be aspects of the local dynamics that cannot be determined from local conditions alone, such as dynamical fluctuations due to wave activity propagating into the column from remote locations. To the extent that such fluctuations influence local diabatic heating rates, their effect should already be included in our parameterized dynamics. To the extent that they do not influence local heating rates, they may be prescribed as external forcing in our coupled SCM, but without the damaging consequences discussed in Sec. 1. Inadequacies of the parameterized dynamics in representing the statistics of local dynamical and thermal variations may thus highlight the need to account for external influences, and may be ameliorated accordingly.

Figure 9 displays amplitude histograms for vertical advection (Figs. 9a,b) and temperature (Fig. 9c,d) fluctuations in the GCM and those derived from the parameterized dynamics given the GCM's heating rates. The amplitudes were calculated at each location as rms deviations from the time-mean, averaged over the troposphere. The gray shaded histograms are for all tropical locations;

the black histograms for convectively active locations only (i.e., the shaded tropical locations in Fig. 8b). Overall, the distributions of the parameterized amplitudes (Figs. 9b,d) of both vertical advection and temperature fluctuations are reasonably similar to their GCM counterparts (Figs. 9a,c), especially in the convective areas. There is, however, a general tendency for parameterized distributions to be narrower than their GCM counterparts, consistent with the neglect of external influences in the dynamical parameterization.

Figure 10 shows lag-correlations of the vertical advection and temperature tendencies with respect to the GCM's diabatic heating rates, averaged over the convectively active locations. Lag-correlations from the parameterized dynamics (dashed lines) reproduce important aspects of those from the GCM (solid lines), including the phase lag of vertical advection with respect to heating, the phase lag of heating with respect to temperature tendencies, and maxima associated with the diurnal cycle (i.e., near ±24 hr). The correlations for the parameterized advection are somewhat too large, which is again consistent with the neglect of external influences in the dynamical parameterization.

The lag-correlations of the GCM's vertical advection and temperature tendencies in Fig. 10 represent systematic relationships with the GCM's diabatic heating. Since the parameterized dynamics are derived from the GCM's diabatic heating, these lag-correlations not only provide a measure with which to evaluate the realism of the parameterized dynamics, they also indicate how closely the parameterized and GCM values *should* match. For example, correlations of hourly GCM and parameterized temperature variations (not shown) are small. However, since the correlations of the GCM's temperature tendencies and diabatic heating are also small for a wide range of lags[1], there is little temperature information in the time-history of diabatic heating, so we do not expect the parameterized dynamics to reproduce the GCM's temperature variations on an hour-by-hour basis.

As a final note, some features of the parameterized dynamics reflect nothing more than the close balance between adiabatic cooling and diabatic heating in the tropics. For example, adiabatic tendencies from a 'perfect balance model' (i.e., obtained by simply setting temperature tendencies to zero, which allows adiabatic and diabatic tendencies to balance perfectly; as in e.g., Sobel and Bretherton 2000) are nearly as accurate as our parameterized tendencies in the tropics in terms of correlations with the GCM's diabatic tendencies (not shown). The crucially important property of our dynamical parameterization is that it produces those high correlations without prescribing an exact balance *a priori* between the adiabatic and diabatic tendencies. Instead, an approximate balance is achieved via a dynamical gravity-wave adjustment model with physically meaningful parameters. Moreover, the parameterized dynamics reproduce dynamical features that the perfect balance model cannot, such as the phase lag of adiabatic tendencies with respect to diabatic tendencies. Perhaps the most impressive aspect of our dynamical parameterization is its ability to produce realistic temperature variations, which are nonexistent in the perfect balance model. Temperature tendencies in our model are calculated as the small difference between the diabatic and parameterized adiabatic tendencies. As a result, even a slightly unrealistic systematic relationship between parameterized advection and diabatic heating rates could permit large and unrealistic temperature deviations to develop, as often seen in SCM integrations (Figs. 1 and 2). The fact that realistic temperature variations are nevertheless produced throughout the tropics by the parameterized dynamics is extremely encouraging in this regard.

---

[1] Correlations were calculated for lags of ±5 days although only values for ±30 hours are shown in Fig. 10.

5. Dynamic stabilization of the SCM

We now investigate the stabilizing influence of the parameterized dynamics on the temperature and humidity variations in the NCAR SCM by comparing error growth in coupled and uncoupled versions of that SCM. These comparisons were performed using the first order model; however, results from the second order model were similar. Given that similarity, we prefer the first order model for its simplicity, its relative insensitivity to the specified horizontal structure, and its improved performance for localized heating (i.e., with a Gaussian horizontal structure; see Fig. 5). Prescribed fields for these comparisons (initial conditions, environmental conditions for the coupled SCM, and advective tendencies for the uncoupled SCM) were obtained from 21 days of 6-hourly observations during TOGA COARE that had been adjusted to balance the mass, moisture, energy, and momentum budgets (J. L. Lin 2002, personal communication; Zhang and Lin 1997).

To incorporate dynamical coupling into the NCAR SCM, the parameters α and τ were chosen based on an effective wavenumber $k_{eff} = 32$. This corresponds to a 400 km Gaussian width (i.e., a 200 km decorrelation length), which is roughly in accord with observed decorrelation lengths for deep tropical convection (e.g., Ricciardulli and Sardeshmukh 2002). At each time-step, the vertical structure of diabatic heating was projected onto the vertical Fourier modes. This requires uniform vertical levels, so the tropospheric levels in the NCAR SCM were altered from their original configuration to be approximately 70 mb thick[2]. Equation (19) was integrated to determine the Fourier transform of vertical temperature advection from which the vertical velocity was calculated. The remaining temperature and moisture advection terms were calculated as discussed in Sec. 2.

We first investigate the influence of coupling on short-term (i.e., 6 hr) error growth by comparing 6-hour temperature changes from the uncoupled SCM (Fig. 1a) to those from the coupled SCM (Fig. 11). To calculate the former (Fig. 1a), 84 separate 6-hour integrations were performed; i.e. one for each of the 84 6-hour segments for which we had access to both initial and final conditions from the TOGA COARE data. Advective tendencies during each of these integrations were held constant at their initial values. Figure 1a displays 6-hour changes contoured as functions of pressure and time. The time axis actually represents separate calculations for the 84 cases in the chronological order that they were observed to occur. In contrast, the six-hour changes from the coupled SCM (Fig. 11) were calculated from a continuous 21-day model run in which temperature and humidity profiles were reset to observed values every 6 hours. This allowed the parameterized advective tendencies to remain consistent with diabatic heating rates throughout the 21-day run after a brief 'spin-up' period. Had the coupled SCM been completely reset every six hours, as the uncoupled SCM, then advection would have had to readjust to diabatic heating, resulting in additional spin-up errors for each 6-hour segment.

Dynamic coupling substantially reduces the 6-hour errors. Six-hour changes from the coupled SCM (Fig. 11) are rarely larger than 1.0 K, whereas the uncoupled SCM (Fig. 1a) produces 6-hour changes exceeding 2.0 K. To be sure, the six-hour temperature changes in the coupled SCM remain larger than observed (Fig. 1b), but are now much more realistic than in the uncoupled SCM. Since dynamical coupling does not affect the physics of NCAR SCM, most of the short-term error growth exhibited by the SCM in Fig. 1a is the *spurious artifact of the decoupled framework and, thus, can obscure errors caused by problematic model physics*.

---

[2] Altering the pressures of vertical levels was found to have only a very small impact on the vertical structure of temperature and humidity produced by the NCAR SCM.

To examine the effect of coupling on the long-term climate and stability of the SCM, control runs and 100-member perturbation ensembles were generated for all 85 sets of observed conditions in the TOGA COARE data. Initial perturbations for the ensemble members were created randomly from uniform distributions of temperature (±1 K) and specific humidity (±10% of the observed specific humidity) at each level – similar to the approach of Hack and Pedretti (2000). In addition, 100-day 'climatological' runs were performed using 3-week averages from the TOGA COARE data to specify the initial conditions, advection for the uncoupled SCM, and environmental conditions for the uncoupled SCM. In all cases, the specified profiles were held fixed during the model runs.

The impact of dynamical coupling on the climate of the SCM is dramatically evident in the vertical profiles of temperature (Fig. 12) and relative humidity (Fig. 13) in the 100-day climatological runs. These figures show 21-day mean errors (solid lines) and standard deviations (dashed lines) from (a) the uncoupled SCM, (b) the coupled SCM, and (c) observations. The model values were obtained from the last 21-days of the integrations, well after the models had reached equilibrium. The SCM climate is vastly improved by coupling. Without coupling, its temperature bias (Fig. 12a) exceeds 5 K throughout the lower troposphere and is nearly 10 K at 750 mb. In contrast, the coupled SCM's temperature errors (Fig. 12b) are typically less than 1.0 K and only exceed 2.0 K at 500 mb. Relative humidity errors are also reduced in the coupled SCM (compare Figs. 13a and 13b). However, humidity errors from both models are constrained by vapor saturation, which caps the growth of those errors.

Variability in both the coupled and uncoupled SCMs is weak, with standard deviations of both temperature (Figs. 12a,b) and humidity (Figs. 13a,b) from the SCMs being much smaller than observed (Fig. 12c, 13c). In fact, all of the model variability in these figures can be attributed to diurnal variations of solar flux. Thus, to utilize this dynamical framework for regional climate modeling, it will be necessary to introduce sources of variability, either in the model physics (e.g., in the form of a stochastic convective parameterization; Lin and Neelin 2002) or that account for remotely forced wave activity propagating into the column (e.g., Mapes 1993).

The growth of ensemble spread is a measure of the stability of the SCM. Figure 14 displays the ensemble spread (averaged over tropospheric levels) for temperature perturbations after four days from each of the 85 sets of ensembles of the uncoupled (gray bars) and coupled SCMs (black bars). The thin horizontal line at 0.58 represents the initial ensemble spread. For 85% of the model runs, ensemble spreads from the coupled SCM are reduced from uncoupled values. In fact, ensemble spread is decreased from its initial value in *all* of the coupled SCM runs, but in only about 50% of the uncoupled runs. That is, dynamical coupling effectively stabilizes the SCM.

6. Summary and conclusions

The decoupling of adiabatic and diabatic tendencies in the traditional SCM framework has a potentially devastating impact on studies that use such models. To investigate and reduce the impact of the decoupling, a simple dynamically coupled SCM has been developed. At any instant, the local vertical velocity in the model is specified by a formula that links the local vertical temperature advection to the evolution of SCM-generated diabatic heating rates up to that instant. This vertical velocity is then used to determine vertical humidity advection, and then horizontal temperature and humidity advection under an additional assumption that the column is embedded in a uniform environment. This coupling strategy allows the SCM to exploit the close relationship between adiabatic and diabatic tendencies to stabilize tropical temperature variations, without an *a priori* imposition of that relationship.

The formula linking vertical advection to the history of column diabatic heating rates is of central importance in this coupled model. Initially, a second order formula, motivated by idealized tropical dynamics and analogous to a damped forced harmonic oscillator, was derived. A first order

formula was also considered in which vertical temperature advection adjusts exponentially to diabatic heating. Parameters in the coupling formulas were determined empirically from the approach to equilibrium of a global dry linear primitive equation model forced by steady diabatic heat sources. To test the parameterized dynamics, the formulas were then used to predict the same model's local response to oscillating heat sources, and found to perform remarkably well, reproducing, for example, the weak dynamical response to fast heating and the phase shift of advection relative to heating for near-resonant heating. Overall, the second order formula was more accurate for globally-coherent heating with sinusoidal zonal structures, but the first order model performed better for more localized heating with Gaussian horizontal structures.

The parameterized dynamics were also tested for their ability to reproduce local vertical advection and temperature variations in a GCM given the time-history of the GCM's local diabatic heating rates. The parameterization works best at tropical locations with active convection. At those locations, the parameterized vertical advection reproduced hour-by-hour fluctuations of the GCM's advection. The parameterized temperature variations did not match the GCM values as accurately. However, such a match is not expected because there is only a weak statistical relationship between local diabatic heating rates and local temperature variations in the GCM itself. More importantly, the parameterized temperature variations did reproduce important statistical properties of GCM's temperature variations in the tropics, including their amplitude and lag-correlation with respect to the diabatic heating.

Dynamical coupling as incorporated in our model also effectively eliminates the spurious instabilities associated with an SCM's artificial decoupling from its environment. This helps the coupled SCM maintain realistic temperature profiles in extended runs. It also reduces short-term error growth and stabilizes the SCM response to initial perturbations, reducing ensemble spread. This stabilization is important because, without it, the physics modules in the SCM generate unrealistic clouds, radiative fluxes, and precipitation from unrealistic thermal structures. In addition, SCM errors that result from or are amplified by the decoupling obscure actual problems with the SCM physics, making it difficult to identify and correct those problems.

Such dynamically coupled SCMs, because they are stable and maintain a realistic climate, also provide us with economical models of regional climate, allowing us to improve upon simple "box"-type models. They should be useful for simulating and understanding in a simple setting, for example, the thermodynamic signatures of remote teleconnections and predictions of regional climate change. Coupled SCMs also have all of the advantages, and few of the disadvantages, of uncoupled SCMs for isolating physical parameterization errors in weather and climate models. In this application, a coupled SCM may be used to simulate regional variations in the full GCM. With an economical replica of the GCM in hand, an extensive investigation of the GCM's sensitivity to changes of model physics becomes possible.

Future efforts to refine the dynamical coupling will enhance its diagnostic utility. In its present form, the coupled SCM lacks high frequency variability. However, the coupled SCM is stable, which means that variability can be introduced through stochastic parameterizations or by specifying external sources of coherent wave-activity without initiating rapid error growth. Finally, we stress that this framework was developed explicitly for tropical conditions. At higher latitudes, Coriolis effects enhance the importance of large-scale dynamics and horizontal advection in the heat and moisture budgets. However, even at high latitudes, there is a strong relationship between vertical velocity and precipitation that could be exploited (e.g., van den Dool 1987, 1990). Incorporating externally forced variations and adapting the dynamical parameterization for higher latitudes are subjects of ongoing research.

a. Acknowledgments

Discussions with B. Mapes, H. van den Dool, and other colleagues at NCAR and CDC were helpful for developing the ideas presented here. Comments by B. Mapes, A. Sobel, and an anonymous reviewer were instrumental in improving the manuscript. B. Stevens, J. Hack, and J. Pedretti provided important assistance with the NCAR SCM. The TOGA COARE dataset was obtained from M. Zhang (at http://atmgcm.msrc.sunysb.edu/iops.html) with the assistance of J. L. Lin. GCM data was provided by S.-I. Shin. This work was partly supported by a grant from the Innovative Research Program, administered by the Cooperative Institute for Research in Environmental Sciences at the University of Colorado.

APPENDIX

Derivation of the second order equation for vertical temperature advection

This Appendix motivates the functional form of the parametric expression for vertical temperature advection X in terms of diabatic heating rate Q. This derivation employs techniques found in textbooks and early papers in atmospheric dynamics and, so, some algebraic details are omitted. What distinguishes this derivation from previous work is that it seeks an explicit expression for the temporal evolution of vertical advection in terms of diabatic heating. We focus on small horizontal scales in the tropics and, so, the effects of the Earth's rotation are neglected. Consider the equations of motion linearized about a motionless basic state with constant temperature lapse rate Γ.

$$\begin{aligned}
&\frac{\partial \mathbf{u}}{\partial t} = -\frac{\nabla p}{\bar{\rho}} - \gamma \mathbf{u} \\
&\nabla \bullet \mathbf{u} = -\frac{\partial w}{\partial z} \\
&\frac{\partial p}{\partial z} = -\rho g \\
&p = \bar{\rho} R T + \rho R \bar{T} \\
&\theta = T\overline{\left(\frac{p_s}{p}\right)^{\kappa}} \\
&\frac{\partial \theta}{\partial t} + X = Q - \gamma \theta \\
&X = w\frac{\partial \bar{\theta}}{\partial z}
\end{aligned} \tag{A.1}$$

where, $\overline{(\ )}$ denotes a basic state quantity and $(\ )_s$ is its value at the surface, γ is a coefficient of linear damping, $\kappa = \frac{R}{c_p}$ is the ratio of the ideal gas constant to the specific heat at constant pressure for dry air, ∇ is the horizontal gradient operator, and $\mathbf{u}$, w, T, ρ, p, are horizontal velocity, vertical velocity, temperature, density, and pressure. The basic state relationships are

$$\begin{aligned}
&\bar{\mathbf{u}} = \bar{w} = 0 \\
&\bar{T} = T_s - \Gamma z \quad . \\
&\bar{p} = p_s\left(\frac{\bar{T}}{T_s}\right)^{\frac{g}{\Gamma R}}
\end{aligned} \tag{A.2}$$

Combining the momentum and continuity equations in (A.1) obtains a relationship between the vertical velocity and pressure.

$$-\left(\frac{\partial}{\partial t} + \gamma\right)\frac{\partial w_n}{\partial z} = -\frac{1}{\bar{\rho}}\nabla^2 p_n = \frac{n^2}{\bar{\rho}} p_n \tag{A.3}$$

where, ψ_n is the horizontal Fourier transform of ψ and n is the total horizontal wavenumber. Combining (A.3) with the linearized ideal gas law in (A.1) yields a relationship between temperature and vertical velocity, which is then converted into an expression for the time derivative of potential temperature in terms vertical velocity.

$$\frac{\partial \theta_n}{\partial t} = -\frac{\bar{\theta}}{n^2 g}\frac{\partial}{\partial t}\left(\frac{\partial}{\partial t}+\gamma\right)\left\{\frac{\partial^2 w_n}{\partial z^2}+\frac{\Gamma}{\bar{T}}\frac{\partial w_n}{\partial z}\right\} \tag{A.4}$$

With $w = 0$ at the surface and the tropopause, the bracketed term in (A.4) can be expressed in terms of its eigenfunctions

$$\begin{aligned}
&\frac{\partial^2 w_m}{\partial z^2}+\frac{\Gamma}{\bar{T}}\frac{\partial w_m}{\partial z} = -\left(m^2+\frac{1}{4h^2}\right)w_m \\
&w_m = e^{-\frac{z}{2h}}\sin(mz) \\
&h = \frac{\bar{T}}{\Gamma} \\
&m = \frac{M\pi}{\Delta z}
\end{aligned} \quad . \tag{A.5}$$

where, M is a positive integer and Δz is the depth of the troposphere. $\bar{T}$ has been treated as a constant in height except for the purposes of differentiation. The thermodynamic relation in (A.1) can now be written as

$$\begin{aligned}
&\frac{\partial^2 X_{mn}}{\partial t^2}+2\gamma\frac{\partial X_{mn}}{\partial t} = -\left(\gamma^2+\sigma_{mn}^2\right)\left(X_{mn}-\alpha_{mn}Q_{mn}\right) \\
&\alpha_{mn} = \frac{\sigma_{mn}^2}{\gamma^2+\sigma_{mn}^2} \\
&\sigma^2 = n^2 g H_m \\
&H_m = \left(m^2+\frac{1}{4h^2}\right)^{-1}\frac{1}{\bar{\theta}}\frac{\partial \bar{\theta}}{\partial z}
\end{aligned} \quad . \tag{A.6}$$

(A.6) has the form of a damped harmonic oscillator forced by a fraction α_{mn} of the diabatic heating rate Q_{mn}.

References

Bergman, J. W., and H. H. Hendon, 2000: Cloud radiative forcing of the low-latitude tropospheric circulation: Linear calculations. *J. Atmos. Sci.*, **57**, 2225-2245

Bergman, J. W. and P. D. Sardeshmukh, 2003 : Usefulness of single column model diagnosis through short-term predictions. *J. Climate*, in press
(available at http: //www.cdc.noaa.gov/~jwb/papers/scm.pdf)

Emanuel, K. A. and M. Zivkovic-Rothman, 1999: Development and evaluation of a convection scheme for use in climate models. *J. Atmos. Sci.*, **56**, 1766-1782

Ghan, S. J., L. R. Leung, and J. McCaa, 1999 : A comparison of three different modeling strategies for evaluating cloud and radiation parameterizations. *Mon, Wea. Rev.*, **127**, 1967-1984

Ghan, S. J. and co-authors, 2000: A comparison of single column model simulations of summertime midlatitude continental convection. *J. Geophys. Res.*, **105**, 2091-2124

Hack, J. J., and J. A. Pedretti 2000: Assessment of solution uncertainties in single-column modeling frameworks. *J. Climate*, **13**, 352-365

Kiehl, J. T., J. J. Hack, G. B. Bonan, B. A. Boville, B. P. Briegleb, D. L. Williamson, and P. J. Rasch, 1996: Description of the NCAR Community Climate Model (CCM3). NCAR Tech. Note NCAR/TN-420+STR, National Center for Atmospheric Research, 152 pp

Lee, W.-H., S. F. Iacobellis, and R. C. J. Somerville, 1997: Cloud radiation forcings and feedbacks: General circulation model tests and observational validation. *J. Climate*, **10**, 2479-2496

Lin, J. W.-B. and J. D. Neelin, 2002 : Considerations for stochastic convective parameterizations. *J. Atmos. Sci.*, **59**, 959-975

Lohmann, U., N. McFarlane, L. Levkov, K. Abdella, and F. Albers, 1999: Comparing different cloud schemes of a single column model by using mesoscale forcing and nudging technique. *J. Climate*, **12**, 438-461

Lord, S. J., 1982: Interaction of a cumulus cloud ensemble with the large-scale environment. Part III: Semi-prognostic test of the Arakawa-Shubert cumulus parameterization. *J. Atmos. Sci.*, **39**, 88-103

Manabe, S. and R. T. Wetherald, 1967: Thermal equilibrium of the atmosphere with a given distribution of relative humidity. *J. Atmos. Sci.*, **24**, 241-259

Mapes, B. E., 1993: Gregarious tropical convection. *J. Atmos. Sci.*, **50**, 2026-2037

Mapes, B. E., 2003: Sensitivities of cumulus ensemble rainfall in a cloud-resolving model with parameterized large-scale dynamics. *J. Atmos. Sci.*, submitted

Moncrieff, M. W., S. K. Krueger, D. Gregory, J.-L. Redelsperger, and W.-K. Tao, 1997: GEWEX Cloud System Study (GCSS) working group 4: Precipitating convective cloud systems. *Bull. Amer. Meteor. Soc.*, **78**, 831-845

Press, W. H., B. P. Flannery, S. A. Teukolsky, and W. T. Vettering, 1989: *Numerical Recipes: The Art of Scientific Computing*. Cambridge Univ. Press, Cambridge, 702 pp

Randall, D. A. and D. G. Cripe, 1999: Alternative methods for specification of observed forcing in single-column models and cloud system models. *J. Geophys. Res.*, **104**, 24 527-24 545

Randall, D. A., K.-M. Xu, R. J. C. Somerville, and S. Iacobellis, 1996: Single-column models and cloud ensemble models as links between observations and climate models. *J. Climate*, **9**, 1683-1697

Randall, D. A. and co-authors, 2003: Confronting models with data: The GEWEX cloud systems study. *Bull. Amer. Meteor. Soc.*, **84**, 455-469

Ricciardulli, L. and P. D. Sardeshmukh, 2002: Local time- and space scales of organized tropical deep convection. *J. Climate*, **15**, 2775-2790

Sobel, A. H. and C. S. Bretherton, 2000: Modeling tropical precipitation in a single column. *J. Climate*. **13**, 4378-4392

Stokes, G. M. and S. E. Schwartz, 1994: The atmospheric radiation measurement (ARM) program: Programmatic background and design of the cloud and radiation test bed. *Bull. Amer. Meteor. Soc.*, **75**, 1202-1221

van den Dool, H. M., 1987: An empirical study on the parameterization of precipitation in a model of the time mean atmosphere. *J. Atmos. Sci.*, **44**, 224-235

van den Dool, H. M., 1990: Time-mean precipitation and vertical motion patterns over the United States. *Tellus.*, **42A**, 51-64

Xie, S. and Co-authors, 2002: Intercomparison and evaluation of cumulus parameterizations under summertime midlatitude continental conditions. *Quart. J. Roy. Meteor. Soc.*, **128**, 1095-1135

Zhang, M. H. and J. L. Lin, 1997: Constrained variational analysis of sounding data based on column-integrated conservations of mass, heat, moisture, and momentum: Approach and application to ARM measurements. *J. Atmos. Sci.*, **54**, 1503-1524

Figure Captions

Fig. 1. 6-hour changes of temperature contoured as functions of pressure and time: (a) simulated by the NCAR SCM and (b) observed during TOGA COARE. The time axis represents 6-hour changes from 84 discrete cases. Contour intervals are 0.3 K; the 0.0 contour is not shown. Dashed contours represent negative values. Fields have been smoothed by one pass of a 1-2-1 filter in the time domain.

Fig. 2. The 21-day mean temperature error for the NCAR SCM forced by observed advective tendencies from TOGA COARE (solid line) and forced by the 21-day mean TOGA COARE advection (short dashed line). The standard deviation of observed temperatures over the 21-day record (long dashed line) is shown for reference.

Fig. 3. Parameters for the formula that links vertical advection to diabatic heating rates as functions of horizontal wavenumber for vertical wavenumbers 1, 4, and 10. Circles represent values of (a) α, (b) γ^{-1} (hours), and (c) σ^{-1} (hours) determined from the PE model forced by steady idealized diabatic heating fields. Dashed lines in (a) and (c) represent analytic estimates from idealized tropical dynamics.

Fig. 4. Parameters for the first-order dynamics as functions of horizontal wavenumber for vertical wavenumbers 1, 4, and 10: (a) α and (b) τ (hours). Dashed lines represent analytic estimates from idealized tropical dynamics. For (b) analytic values correspond to the intrinsic gravity wave frequency.

Fig. 5. Rms vertical advection errors normalized by the rms heating amplitude for parameterized dynamics compared to the local response of the linear PE model to oscillating heating for a wide range of frequencies and vertical wavenumbers. Shown are errors for: (a) the second order dynamics using heating with a wavy zonal structure, (b) the second order dynamics using heating with a Gaussian zonal structure, and (c) first order dynamics using a Gaussian zonal structure. The plotting scales are linear for errors less than 1.0 and is logarithmic for errors greater than 1.0. Rms errors are calculated from the tropospheric response below 300 mb to reduce corruption by vertically-propagating waves.

Fig. 6. Comparisons of the parameterized dynamics (right panels) to the response of the PE model (left panels) to resonant heating (12-hour period) as functions of phase and pressure: (a) Vertical advection from the PE model forced by heating with a wavy zonal structure, (b) vertical advection from the PE model forced by heating with a Gaussian zonal structure, (c) vertical advection from the second order parameterized dynamics, and (d) vertical advection from the first order parameterized dynamics. Phase is shown relative to the maximum heating rate (5 K day^{-1}). Contour intervals are 5.0 K day^{-1} for (a) and (b) and 0.6 K day^{-1} for (c) and (d).

Fig. 7. Vertical advection from (a) the GCM and (b) from the parameterized dynamics as a function of time (days) and pressure (mb) for a convectively-active location in the equatorial west Pacific. Contour intervals are 2.0 K day^{-1}.

Fig. 8. Maps of (a) correlations between tropospheric vertical advection from the GCM and parameterized values and (b) GCM diabatic heating rates. Contour intervals are 0.1 in (a) and 0.5 K day^{-1} in (b). For clarity, values less that 0.5 are not contoured in either (a) or (b).

Fig. 9. Amplitude histograms for variations at tropical locations: (a) Vertical advection from the GCM, (b) parameterized vertical advection, (c) temperature from the GCM, and (d) parameterized temperature. Bars represent the total area of grid boxes with values within a given a range of amplitudes normalized by the total area of the tropics. Gray bars represent values sampled from all tropical locations. Black bars represent values sampled from convectively active tropical locations.

Fig. 10. Lag-correlations for vertical advection (top pair of lines) and temperature tendency (bottom pair) with respect to GCM diabatic heating rates as a function of lag (hr), averaged over tropical locations with active convection. Solid lines indicate GCM values and dashed lines indicate parameterized values.

Fig. 11. 6-hour changes of temperature from the coupled SCM contoured as a function of pressure and time. This figure can be compared to the 6-hour changes from the uncoupled SCM in Fig. 1a to determine the impact of decoupling on error growth. The time axis represents 6-hour changes from 84 discrete cases. Contour intervals are 0.3 K; the 0.0 contour is not shown. Dashed lines represent negative values. Fields have been smoothed by one pass of a 1-2-1 filter in the time domain.

Fig. 12. 21-day mean temperature errors (solid lines) and standard deviations (dashed lines) from (a) the uncoupled SCM, (b) the coupled SCM, and (c) observations. SCM errors are determined from the last 21 days of 100-day runs using time-mean forcing from TOGA COARE.

Fig. 13. 21-day mean relative humidity errors (solid lines) and standard deviations (dashed lines) from (a) the uncoupled SCM, (b) the coupled SCM, and (c) observations.

Fig. 14. Ensemble spread of temperature at 4 days averaged over the troposphere for 85 ensembles of the uncoupled SCM (gray bars) and the coupled SCM (black bars). The thin horizontal line represents the initial ensemble spread.

(a) SCM

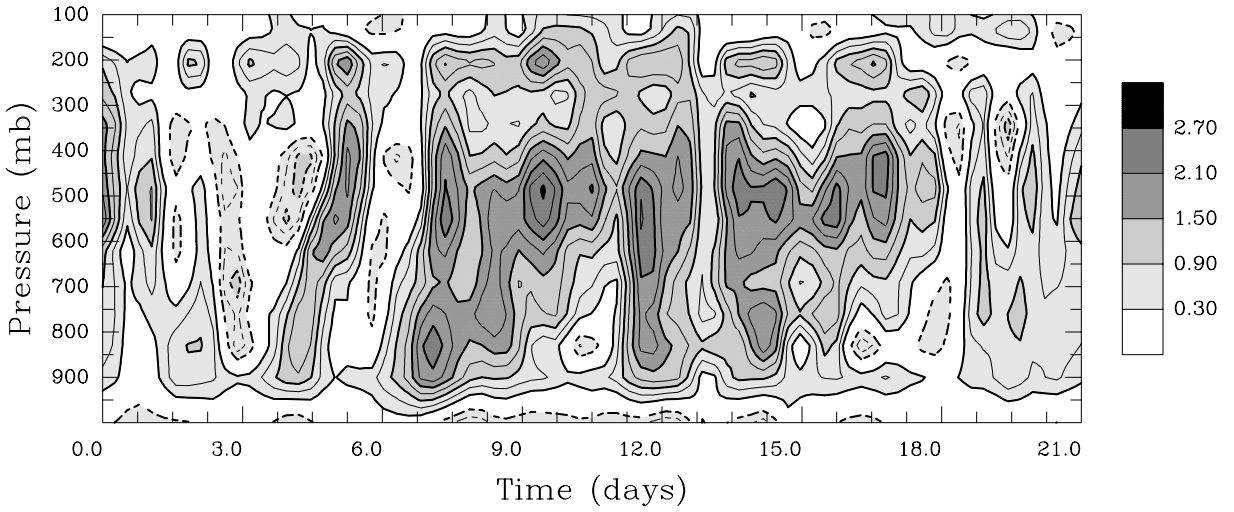

(b) Observations

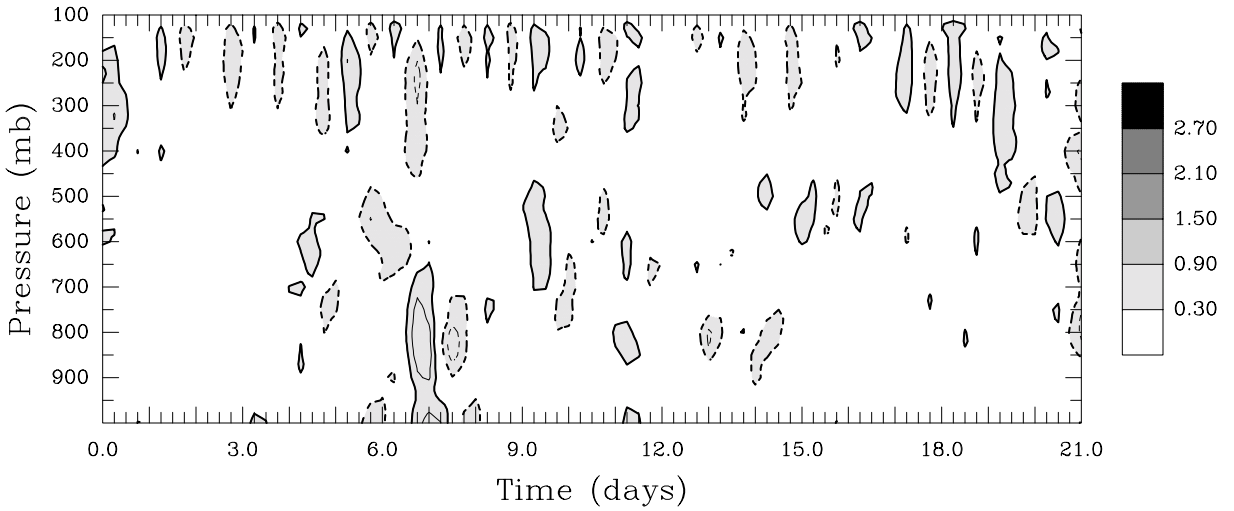

Fig. 1: 6-hour changes of temperature contoured as functions of pressure and time: (a) simulated by the NCAR SCM and (b) observed during TOGA COARE. The time axis represents 6-hour changes from 84 discrete cases.

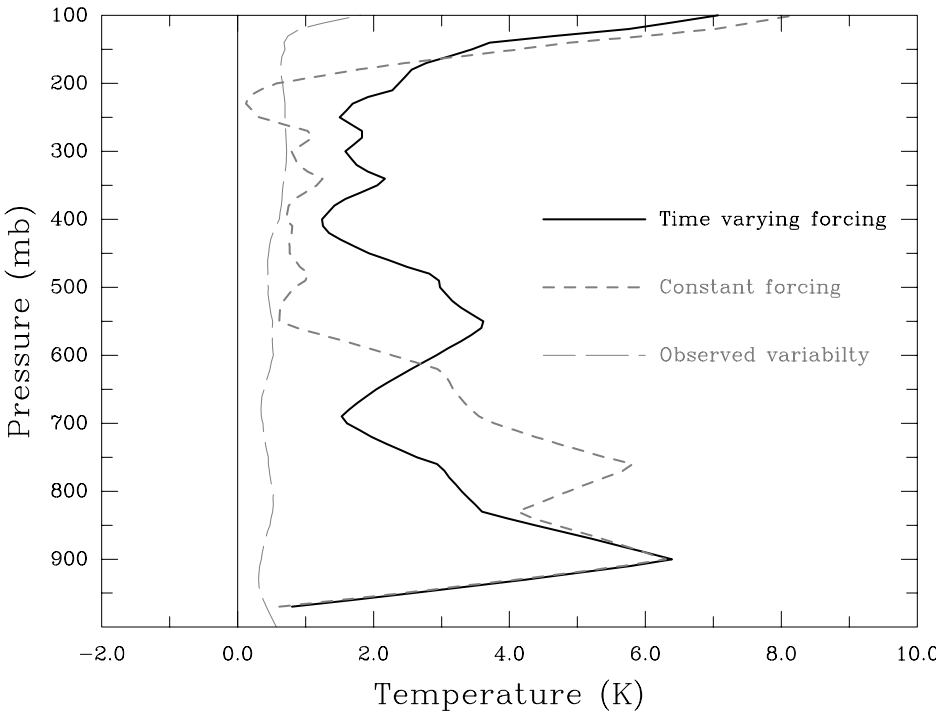

Fig. 2: 21-day mean temperature errors from the NCAR SCM: forced by advective tendencies from TOGA COARE (solid line) and forced by the 21-day averaged advective tendencies (short-dashed line). The standard deviation of observed temperature over the 21-day record(long dashed line) is shown for reference.

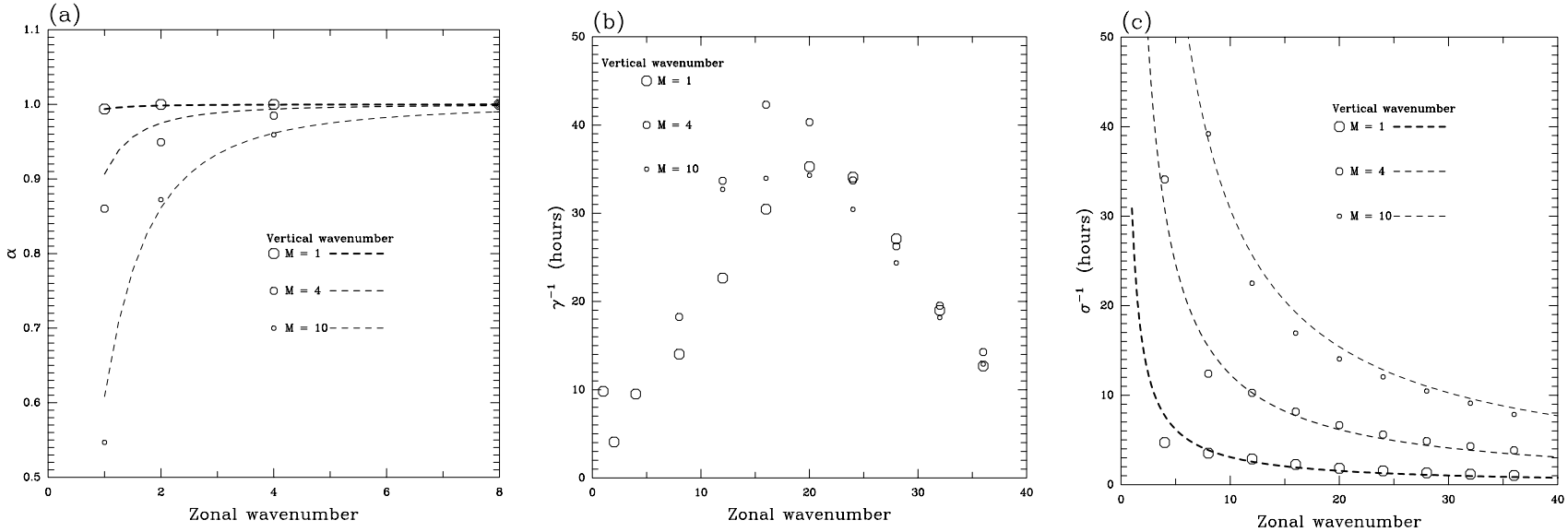

Fig. 3: Parameters for the formula that links vertical advection to diabatic heating rates. Circles represent values determined from the PE model forced by steady idealized heating fields. Dashed lines in (a) and (b) represent analytic estimates from idealized tropical dynamics.

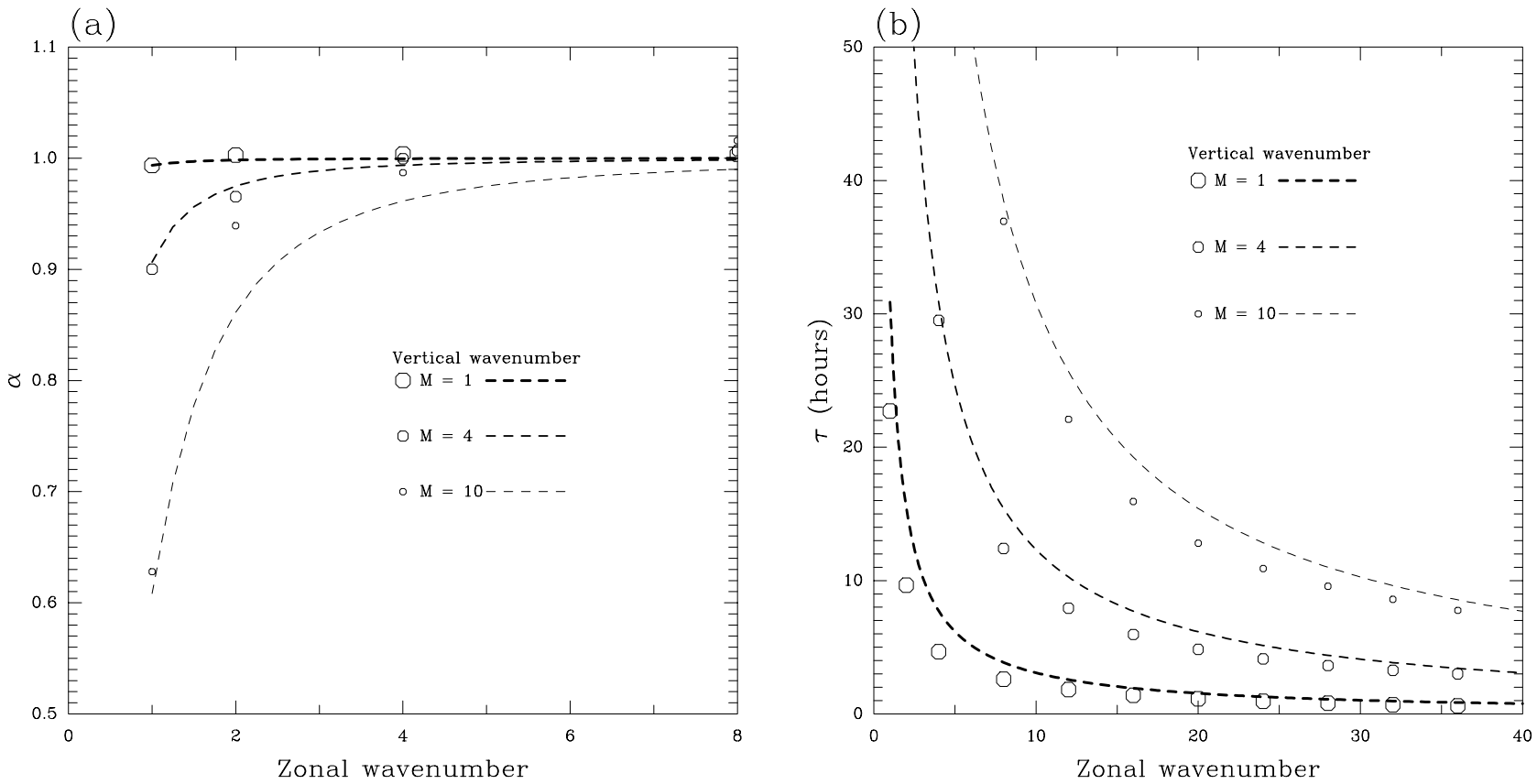

Fig. 4: Parameters for the first-order dynamics as functions of horizontal wavenumber for vertical wavenymbers 1, 4, and 10. Dashed lines represent analytic estimates from idealized tropical dynamics. For (b) analytic values correspond to the gravity wave timescale.

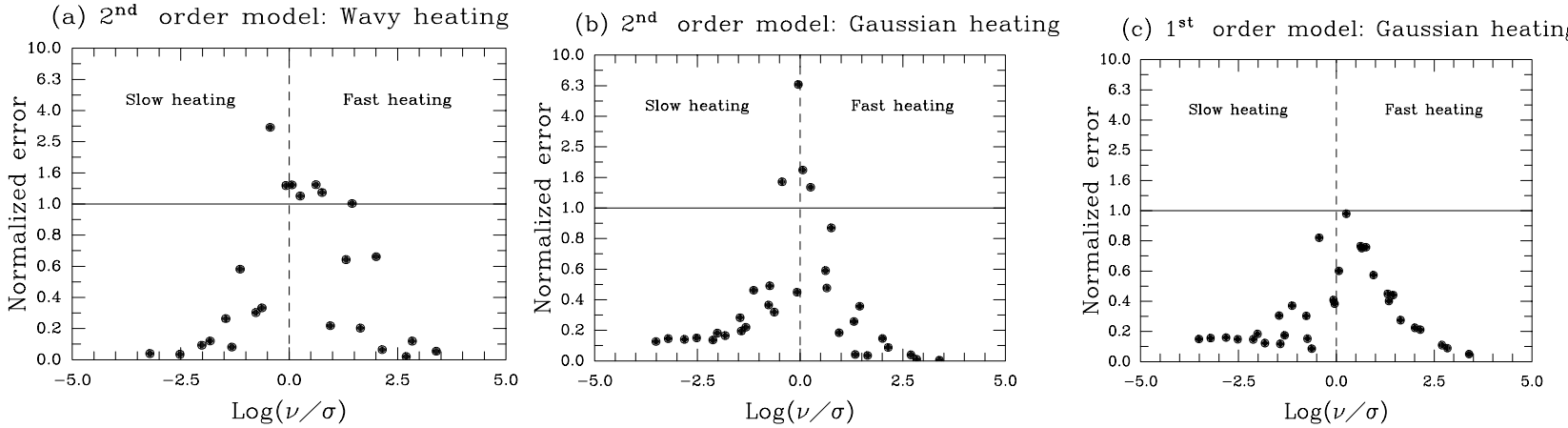

Fig. 5: Absolute rms errors (normalized by the amplitude of the heating rate) for the parameterized vertical advection compared to the response of the linear PE model to oscillating heating for a wide range of frequencies and vertical wavenumbers. Shown are errors for: (a) the 2nd order model for heating with a wavy zonal structure, (b) the 2nd order model for heating with a Guassian (i.e., localized) zonal structure, and (c) the 1st order model for heating with a Gaussian zonal structure.Errors are calculated over tropospheric levels below 300 mb to avoid corruption by vertically propagating waves.

(a) Primitive equation model: Wavy heating

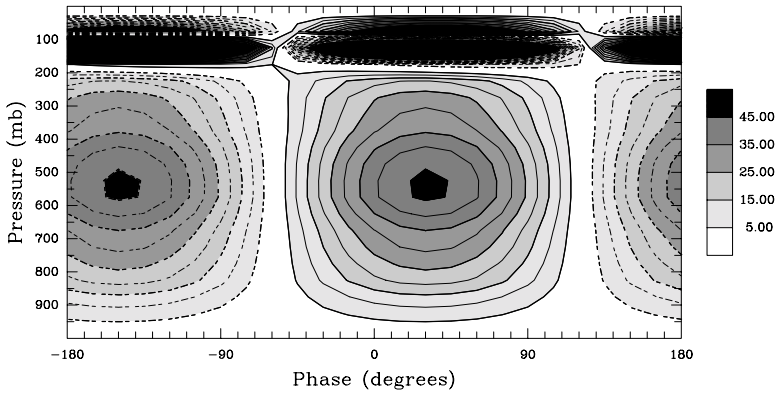

(c) Second order parameterized dynamics

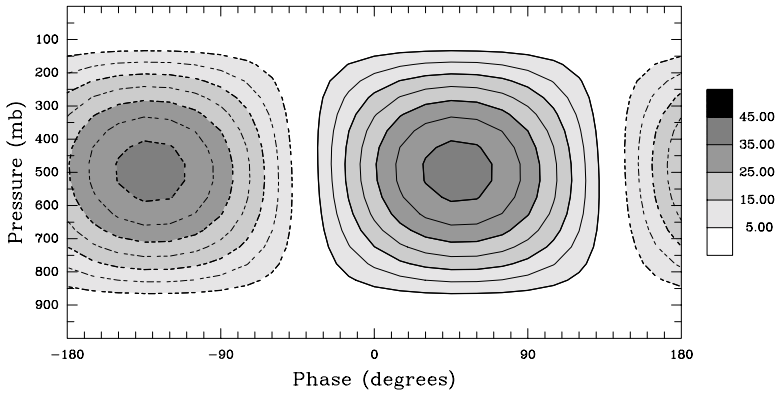

(b) Primitive equation model: Gaussian heating

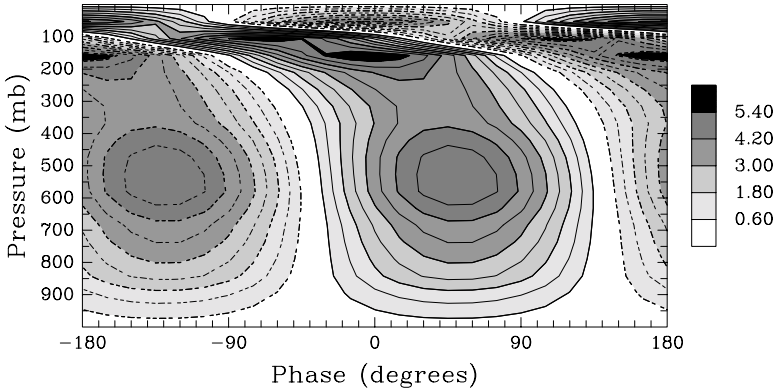

(d) First order parameterized dynamics

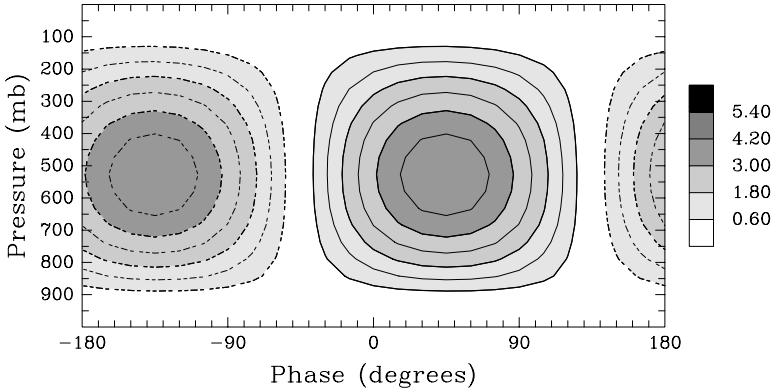

Fig. 6: Comparisons of the parameterized dynamics (right panels) to the response of the PE model (left panels) to resonant heating (12-hour period). Shown are vertical advection as a function of phase of the oscillation and pressure. Phase is shown relative the the time of maximum heating (5 K day^{-1}).

(a) GCM vertical advection

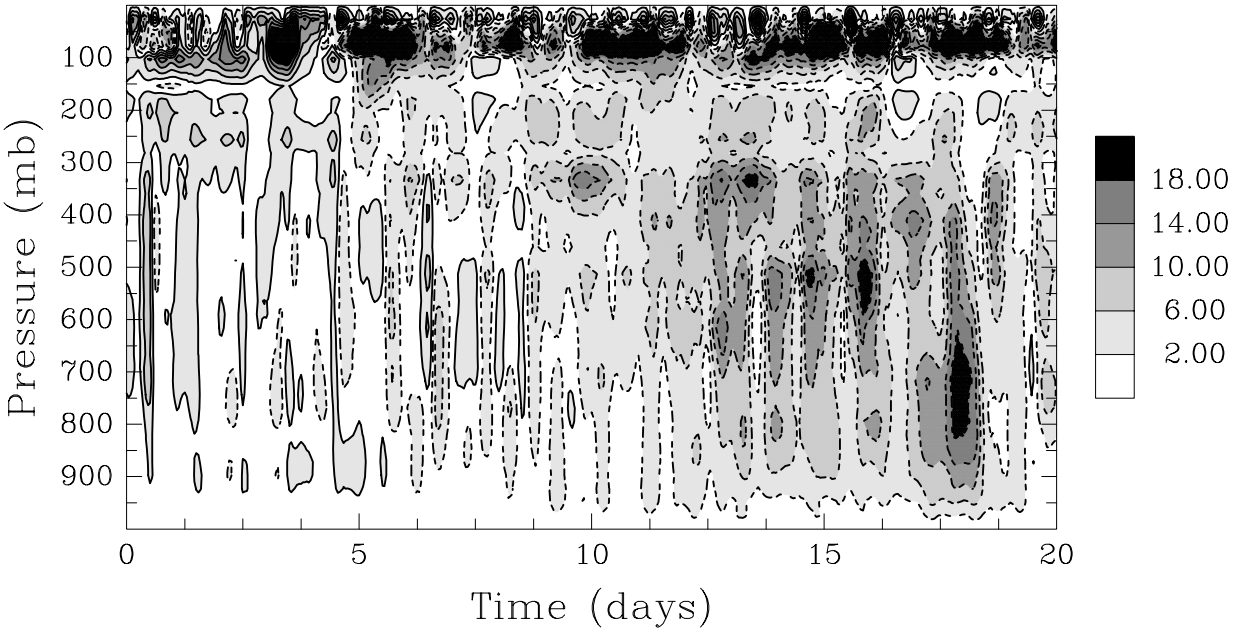

(b) Parameterized vertical advection

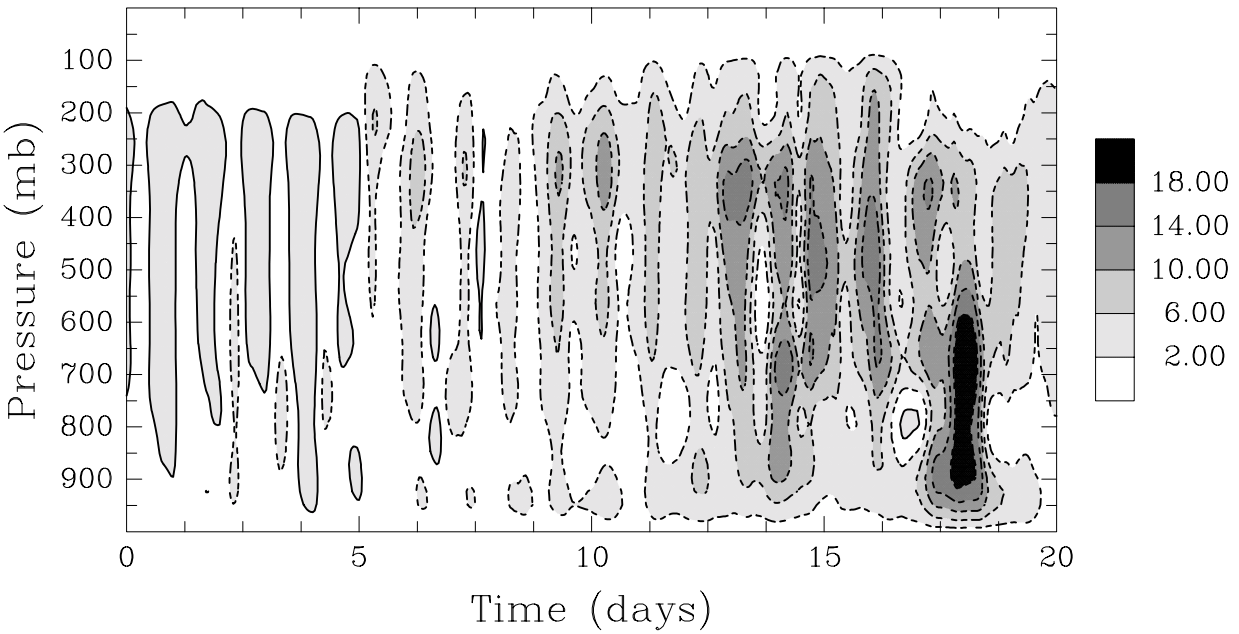

Fig. 7. Vertical advection from (a) the GCM and (b) from the parameterized dynamics as a function of time (days) and pressure (mb) for a convectively active location in the equatorial west Pacific.

(a) Correlation: GCM vs. parameterized vertical advection

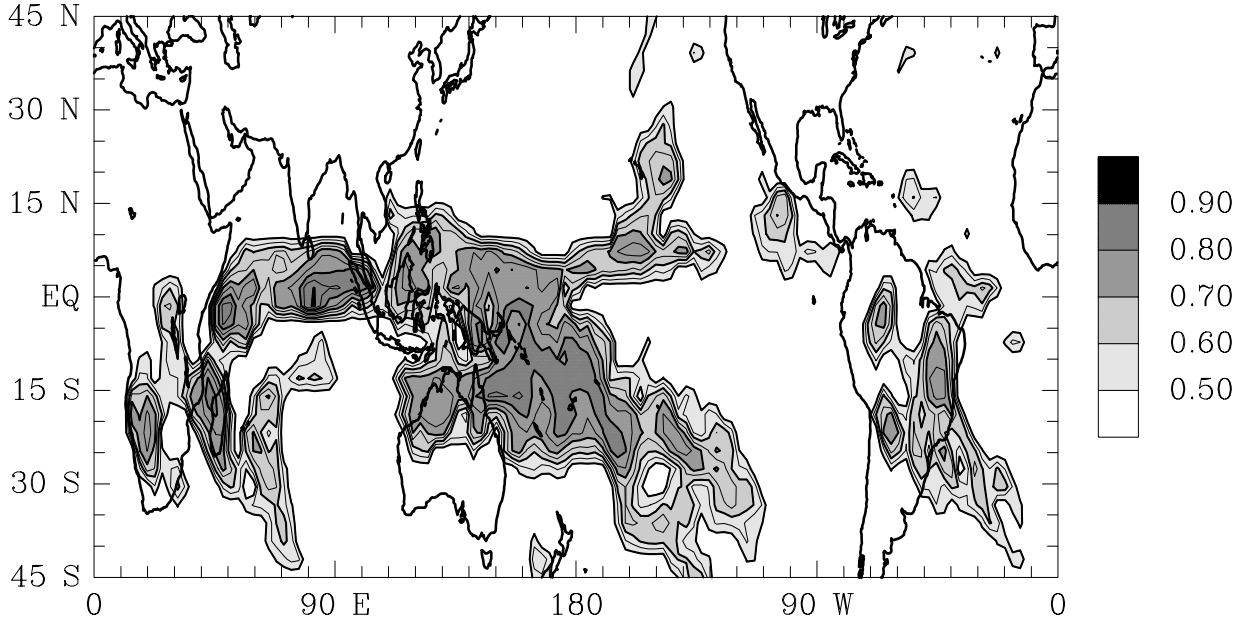

(b) GCM diabatic heating

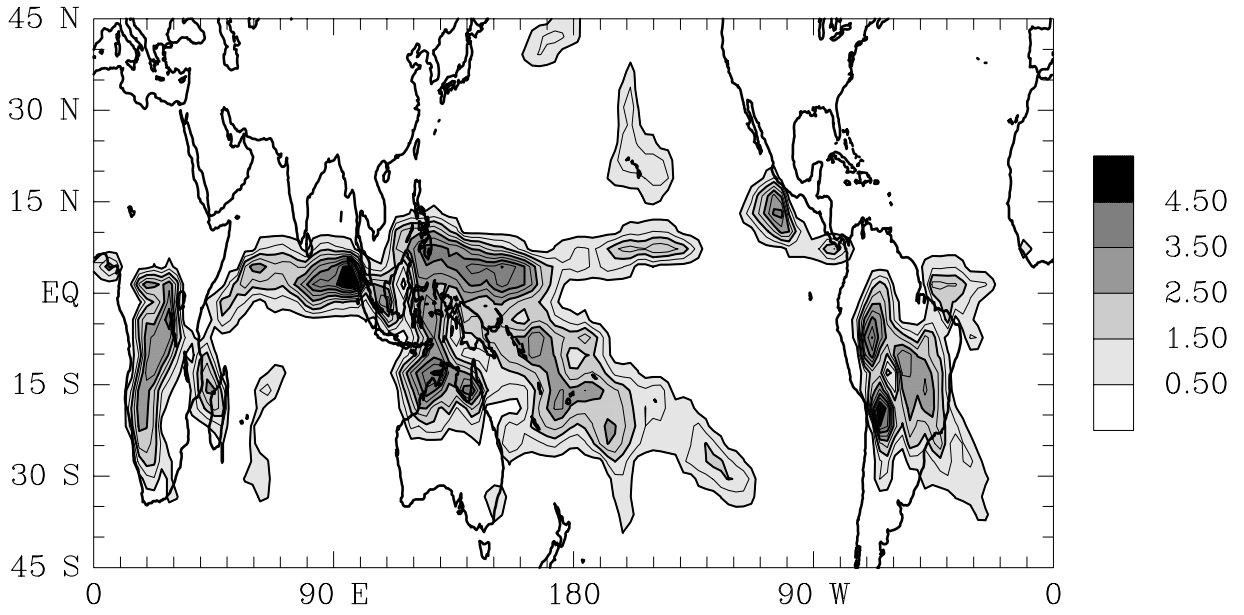

Fig. 8. Maps of (a) correlations between tropospheric vertical advection from the GCM and parameterized values and (b) GCM diabatic heating rates.

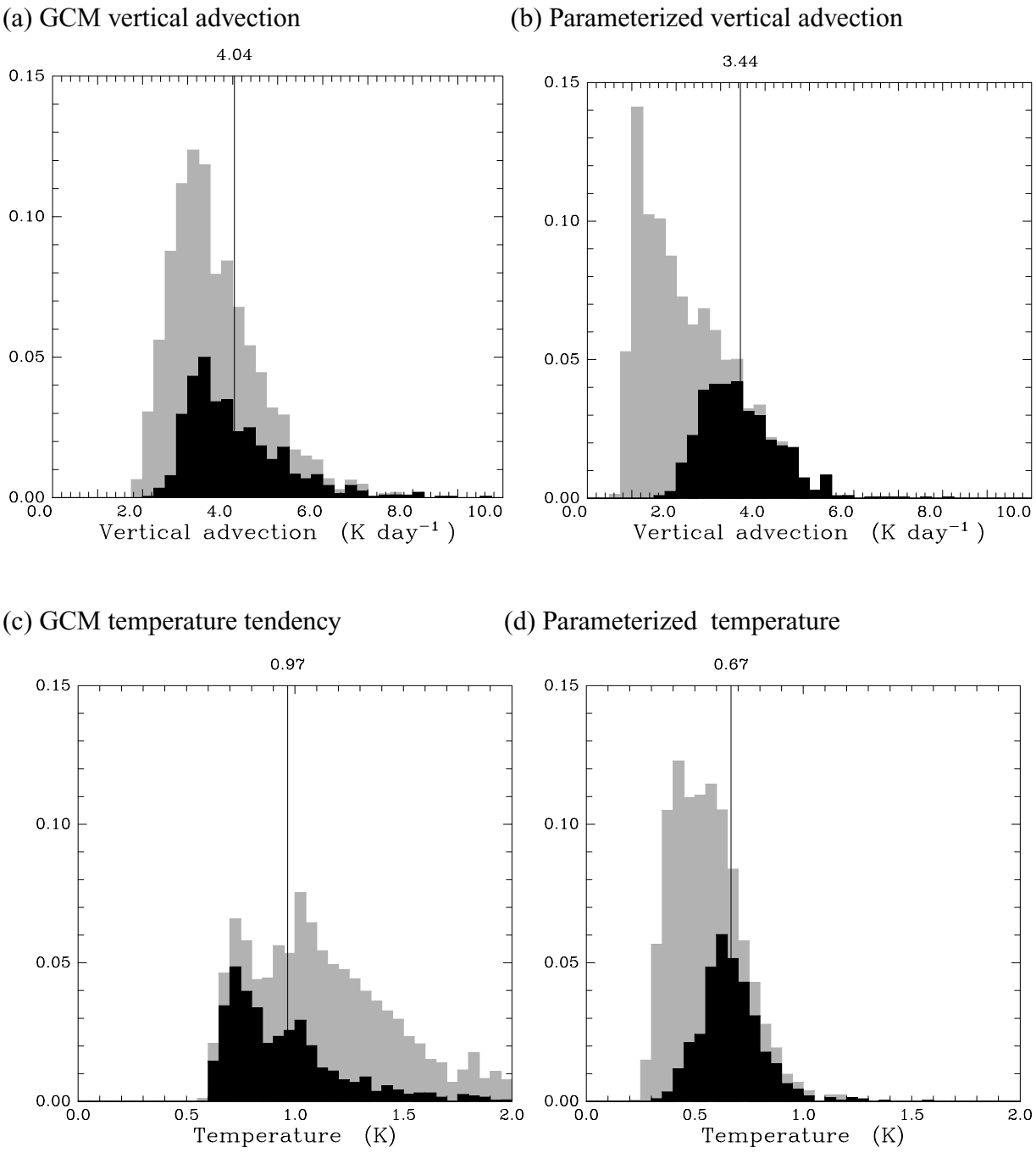

Fig. 9. Amplitude histograms for variations at tropical convections: (a) Vertical advection from the GCM, (b) parameterized vertical advection, (c) temperature from the GCM, and (d) parameterized temperature. Bars represent the total area of grid boxes with values within a given range of amplitude normalized by the total area of the tropics. Gray bars represent values sampled from all tropical locations. Black bars represent values sampled from convectively active tropical locations.

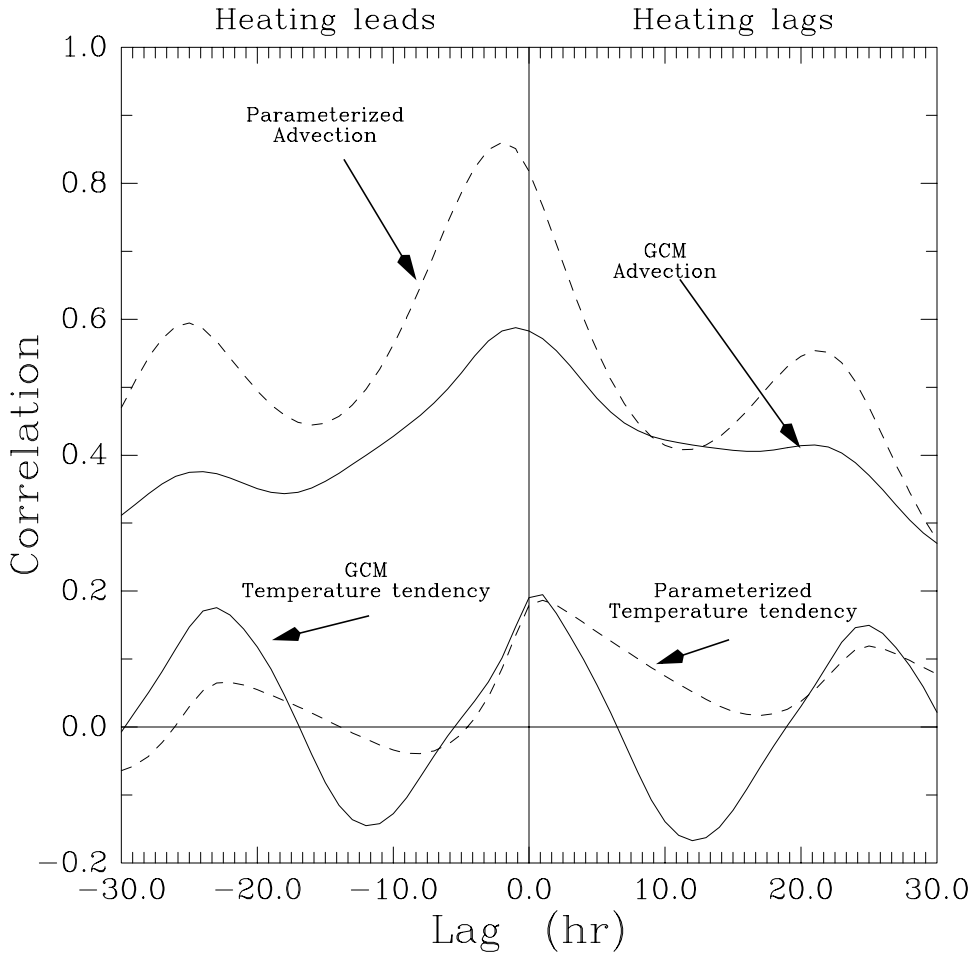

Fig. 10: Lag correlations of vertical advection (top pair of lines) and temeprature tendency (bottom pair) with respect to GCM heating rates averaged over locations of active tropical convection. Values from parameterized dynamics are shown with dashed lines. GCM values are shown with solid lines.

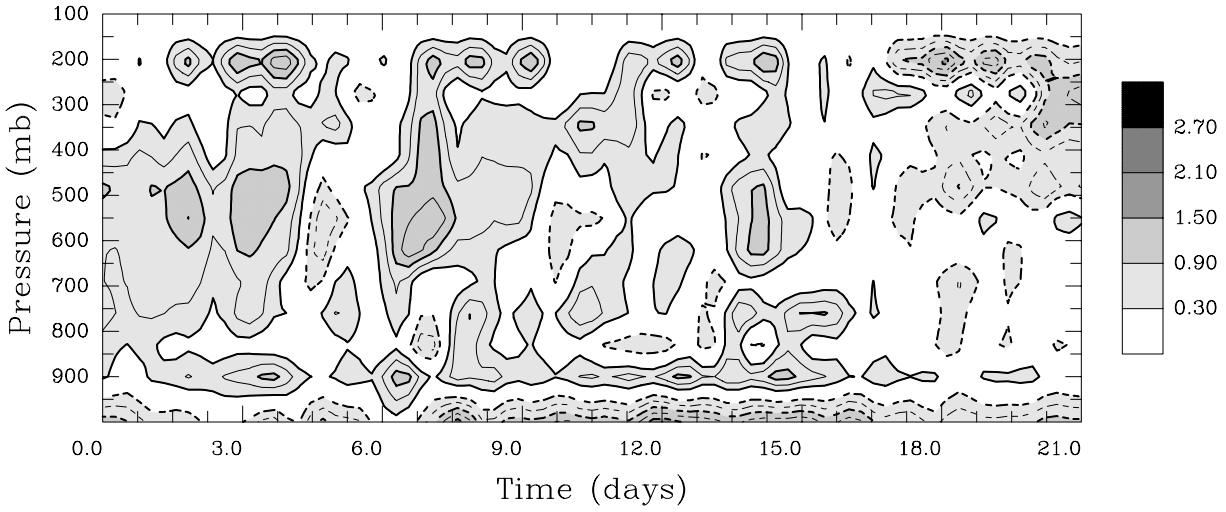

Fig. 11: 6 hour changes of temperature from the coupled SCM countoured as a function of pressure and time.

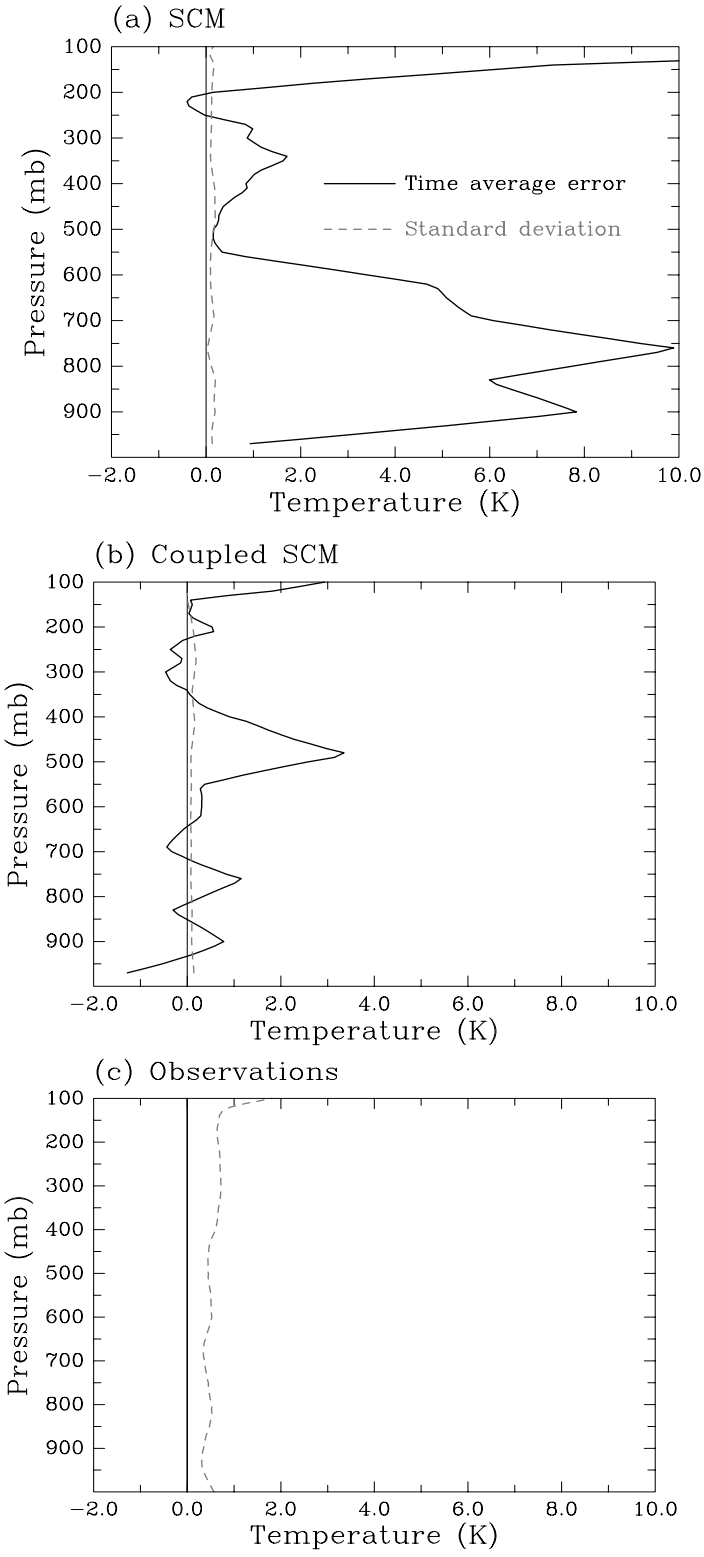

Fig. 12: 21-day mean temperature errors (solid lines) and standard deviations (dashed lines) from (a) the uncoupled SCM, (b) the coupled SCM, and (c) from observations.

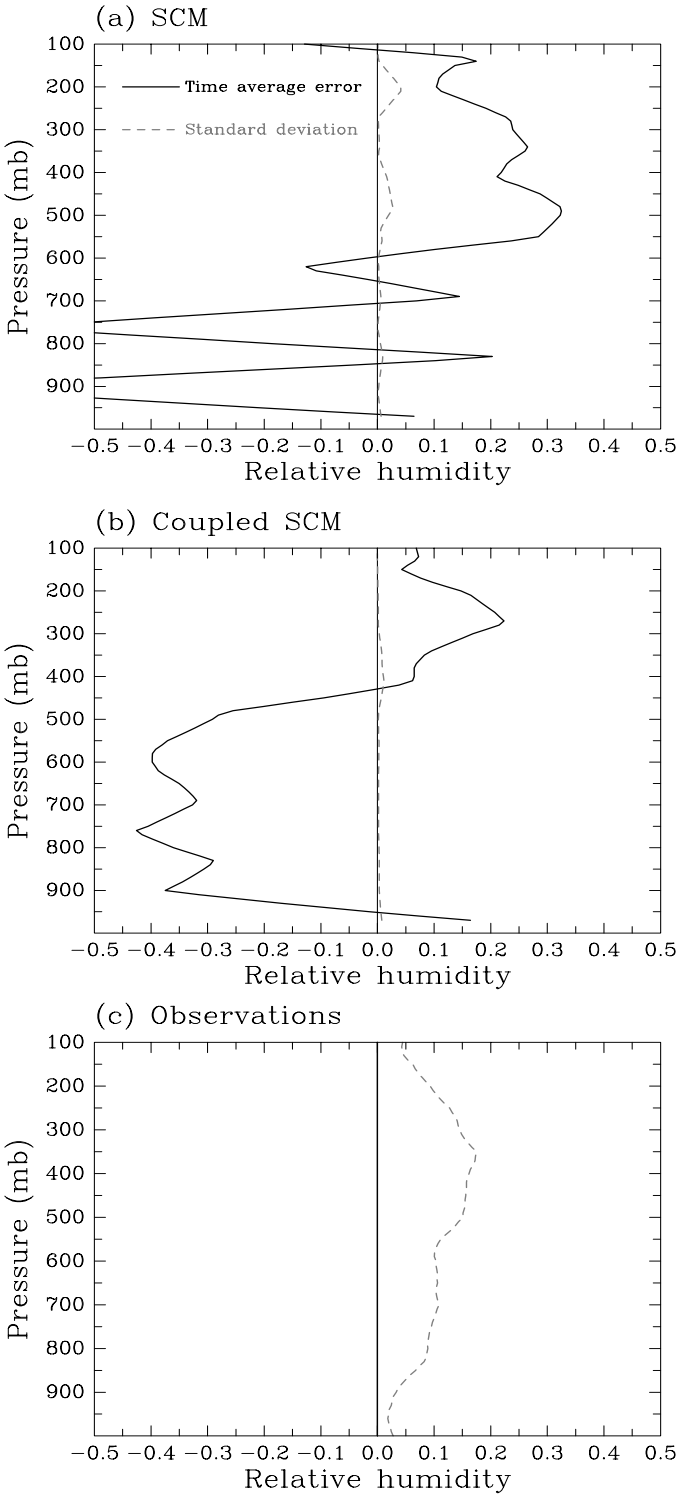

Fig. 13: 21-day mean relative humidity errors (solid lines) and standard deviations (dashed lines) from (a) the uncoupled SCM, (b) the coupled SCM, and (c) from observations.

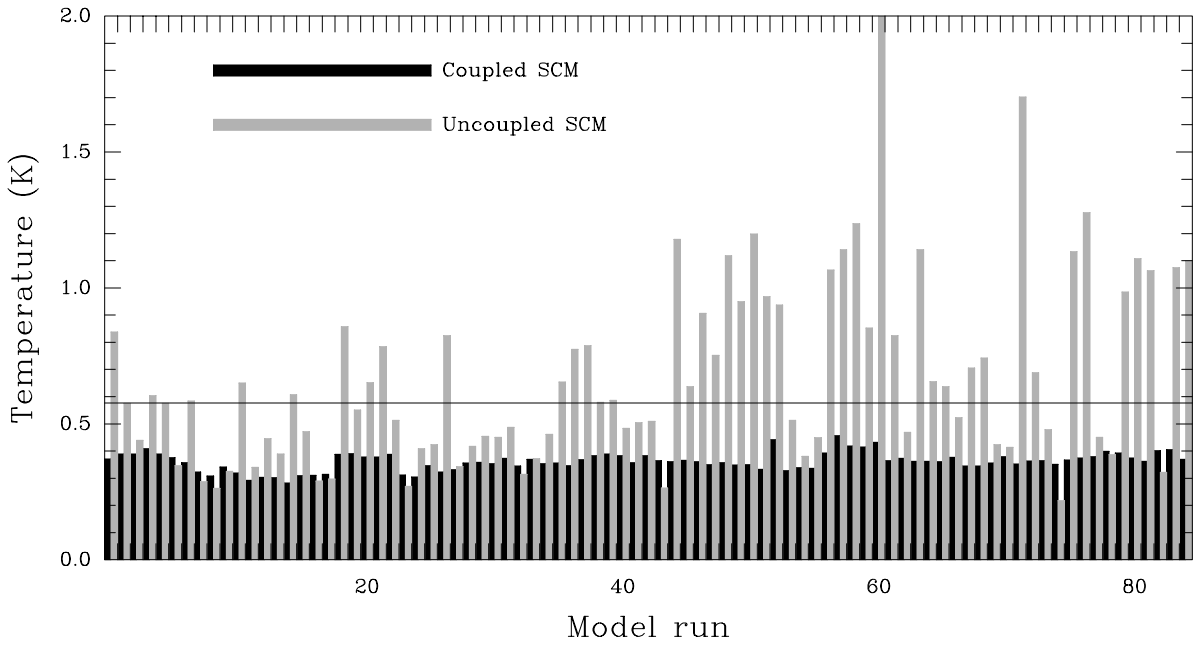

Fig. 14: Ensemble spread of temperature at 4 days averaged over the troposphere for 85 ensembles of the uncoupled SCM (gray bars) and of the coupled SCM (black bars). The thin horizontal line represents the initial ensemble spread.